

Superdirective Antenna Pairs for Energy-Efficient Terahertz Massive MIMO

Konstantinos Dovelos, Stylianos D. Assimonis, Hien Quoc Ngo, *Senior Member, IEEE*, and Michail Matthaiou, *Fellow, IEEE*

Abstract—Terahertz (THz) communication is widely deemed the next frontier of wireless networks owing to the abundant spectrum resources in the THz band. Whilst THz signals suffer from severe propagation losses, a massive antenna array can be deployed at the base station (BS) to mitigate those losses through beamforming. Nevertheless, a very large number of antennas increases the BS’s hardware complexity and power consumption, and hence it can lead to poor energy efficiency (EE). To surmount this fundamental problem, we propose a novel array design based on superdirectivity and nonuniform inter-element spacing. Specifically, we exploit the mutual coupling between closely spaced elements to form superdirective pairs. A unique property of them is that all require the same excitation amplitude, and thus can be driven by a single radio frequency chain akin to conventional phased arrays. Moreover, they facilitate multi-port impedance matching, which ensures maximum power transfer for any beamforming angle. After addressing the implementation issues of superdirectivity, we show that the number of BS antennas can be effectively reduced without sacrificing the achievable rate. Simulation results demonstrate that our design offers huge EE gains compared to uncoupled arrays with uniform spacing, and hence could be a radical solution for future THz systems.

Index Terms—Antenna arrays, channel estimation, energy efficiency, hybrid beamforming, impedance matching, mutual coupling, superdirectivity, THz communications.

I. INTRODUCTION

Massive multiple-input multiple-output (MIMO) is now a mature technology, which has been adopted by 5G new radio to provide superior network capacity and coverage. In parallel, millimeter wave (mmWave) systems start gaining ground as an effective way for delivering multi-gigabit rates thanks to their very large bandwidths [1], [2]. Toward this direction, communication above 100 GHz, i.e., terahertz (THz) frequencies, is widely deemed the next frontier of wireless systems with a plethora of promising applications, ranging from ultra-broadband femtocells to terabit-per-second links for wireless backhaul [3]. Nevertheless, THz signals are subject to severe propagation and molecular absorption losses, which can drastically limit the communication range and coverage [4]. To deal with this problem, large antenna arrays can be deployed at the base station (BS) to increase the signal power by means of sharp beamforming. As a result, massive MIMO is expected to be an integral component of future THz systems [5]. On

the other hand, THz radio frequency (RF) circuits, e.g., power amplifiers, phase shifters, etc., exhibit significantly higher power consumption than their sub-6 GHz counterparts [6]. Additionally, baseband processing with multiple RF chains during channel estimation and data transmission is power intensive [7]. In conclusion, achieving a large beamforming gain in an energy efficient manner constitutes a major engineering challenge which calls for novel solutions.

The beamforming capabilities of multi-antenna systems have been extensively investigated in the past. For example, a typical N -element phased array offers a gain that scales linearly with N when maximum ratio transmission (MRT) is used [8]. However, higher gains are possible by leveraging the mutual coupling between adjacent antennas. Specifically, Uzkov theoretically proved in his seminal work [9] that a uniform linear array (ULA) of N isotropic radiators and vanishingly small inter-element spacing has an endfire directivity of N^2 , a phenomenon now known as *superdirectivity*.

The theme of superdirectivity has been widely studied from both information theoretic and pure electromagnetic standpoints, e.g., [10]–[17], and references therein. However, most of the related literature considers arrays of uniform spacing. More importantly, it overlooks various communication and practical aspects, such as the EE, implementation limitations in hybrid analog-digital architectures, and channel estimation performance. Consequently, there are still critical questions about how THz massive MIMO could fully benefit from superdirectivity. Regarding other approaches, there is a stream of recent papers on arrays-of-subarrays (AoSA) with metallic antennas [18]–[20] and graphene-based plasmonic nanoantennas [21], [22], as well as on intelligent reflecting surfaces [23], [24], which can improve the EE of the system. Yet, they neglect the superdirective effects of closely spaced BS antennas.

This paper aims to show that superdirectivity can be ingeniously used to reduce the hardware complexity and boost the EE of THz massive MIMO. The contributions of our work are summarized as follows:

- We introduce a coupling-aware array model based on *antenna theory*. In particular, we derive the input impedance matrix of the BS array assuming lossy dipole antennas. Note that directional antennas, such as linear dipoles, are mutually coupled even for half-wavelength spacing. Therefore, proper characterization of their electromagnetic interaction is crucial to beamforming [25].
- Based on the introduced array model, we study the implementation issues of superdirectivity. In particular,

Manuscript received July 1, 2022; revised December 19, 2022, May 6, 2023, and August 8, 2023; accepted August 22, 2023.

Konstantinos Dovelos is with Meta Materials, Inc., Athens, Greece, email: kostis.dovelos@metamaterial.com. All other authors are with the Centre for Wireless Innovation, Queen’s University Belfast, Belfast BT3 9DT, U.K., email: {s.assimonis, hien.ngo, m.matthaiou}@qub.ac.uk.

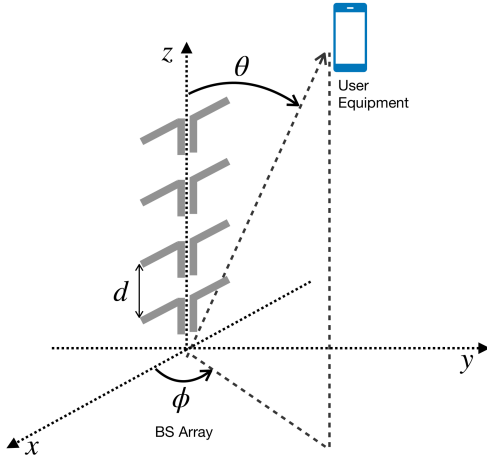


Fig. 1: Illustration of the antenna array considered at the BS.

we look into the impedance matching problem as well as the realization of superdirective beamsteering in a hybrid analog-digital array architecture. We address both problems by proposing a novel array design relying on coupled antenna pairs. Specifically, the BS array is divided into multiple two-element groups, which are adequately separated so that inter-group coupling can be neglected. The resulting nonuniform linear array (NULA) greatly simplifies the optimal multi-port matching, and more importantly, requires uniform amplitude excitation. Consequently, it can be driven by a single RF chain to produce a pencil-like beam, similar to conventional phased arrays. The presented structure is also extended to the nonuniform planar array (NUPA) case. It is worth stressing that our method can be readily applied to an AoSA, wherein each subarray is a NULA or a NUPA.

- We exploit the excessive power gain of the proposed design to decrease the number of BS antennas. This leads to a low-dimensional massive MIMO system, whose performance is assessed in terms of the achievable rate under perfect and imperfect channel state information (CSI). For this purpose, approximate closed-form expressions for the signal and interference powers are provided assuming MRT. Moreover, the channel estimation problem is addressed by leveraging the popular orthogonal matching pursuit (OMP) algorithm.
- Extensive simulation results are provided corroborating our analysis. In particular, it is demonstrated that the proposed array design boosts the EE of THz massive MIMO without sacrificing the data transmission and channel estimation performances. As such, it has the potential to realize low-complexity and energy-efficient MIMO arrays with sharp beamforming capabilities.

The rest of the paper is organized as follows: Section II delineates the BS array model. Section III presents the impedance matching problem. Section IV delves into the implementation issues of superdirectivity and details the proposed solution. Section V introduces the system model used for performance evaluation. Section VI analyzes the signal and interference powers under the proposed array. Section VII addresses the

TABLE I
MAIN NOTATION USED IN THIS WORK

Notation	Description
N	Number of BS antennas
d	Inter-element spacing in ULA
N_g	Number of antenna groups in NULA
\bar{N}	Number of antennas per group in NULA
d_g	Inter-group spacing
\bar{d}	Inter-element spacing within each antenna group
f, λ, κ	Carrier frequency, wavelength, wavenumber
ℓ, ρ	Dipole length, radius
η, μ	Free-space impedance, permeability
σ_c	Copper conductivity
$\mathbf{Z}_{\text{ideal}}$	Input impedance matrix for lossless dipoles
\mathbf{Z}	Input impedance matrix for lossy dipoles

channel estimation problem. Section VIII explains how to reduce the number of BS antennas. Section IX is devoted to numerical simulations. Finally, Section X summarizes the main conclusions of this work.

Notation: Throughout the paper, $D_N(x) = \frac{\sin(Nx/2)}{N \sin(x/2)}$ is the Dirichlet sinc function; $\mathbf{A}(\cdot, \cdot, \cdot)$ is a vector field; \mathbf{A} is a matrix; \mathbf{A}^* , \mathbf{A}^\dagger , \mathbf{A}^H , and \mathbf{A}^T are the conjugate, pseudoinverse, conjugate transpose, and transpose of \mathbf{A} , respectively; $[\mathbf{A}]_{i,j}$ is the (i, j) th entry of \mathbf{A} ; $\mathbf{A}(i)$ is the i th column of \mathbf{A} ; $\text{blkdiag}(\mathbf{A}_1, \dots, \mathbf{A}_n)$ is a block diagonal matrix; \mathbf{a} is a vector; $\|\mathbf{a}\|_1$ and $\|\mathbf{a}\|$ are the l_1 -norm and l_2 -norm of \mathbf{a} , respectively; $\text{mag}(\mathbf{a}) = [|a_1|, \dots, |a_N|]^T$ for $\mathbf{a} = [a_1, \dots, a_N]^T$; $\mathbf{1}_{N \times M}$ is the $N \times M$ matrix with unit entries; \mathbf{I}_N is the $N \times N$ identity matrix; $\mathbf{0}_{N \times M}$ is the $N \times M$ matrix with zero entries; \otimes denotes the Kronecker product; $\mathbf{a} \cdot \mathbf{b}$ is the inner product between \mathbf{a} and \mathbf{b} ; $\mathbb{E}\{\cdot\}$ denotes expectation; $\mathcal{CN}(\boldsymbol{\mu}, \mathbf{R})$ is a complex Gaussian vector with mean $\boldsymbol{\mu}$ and covariance matrix \mathbf{R} . Finally, $\text{Re}\{\cdot\}$ and $\text{Im}\{\cdot\}$ are the real and imaginary parts of a complex variable, respectively.

II. ANTENNA ARRAY MODEL

In this section, we present the BS array model which takes into account antenna mutual coupling.

A. Radiated Power

Consider an N -element ULA along the z -axis at the BS, as depicted in Fig. 1.¹ The inter-element spacing is d . Each element is a linear dipole parallel to the x -axis, and is of length ℓ and radius ρ . According to [26, Ch. 4], the current distribution on each dipole n has approximately the sinusoidal form

$$I_n(x') \approx I_n(0) \frac{\sin(\kappa\ell/2 - \kappa|x'|)}{\sin(\kappa\ell/2)}, \quad |x'| \leq \ell/2, \quad (1)$$

where $I_n(0) \in \mathbb{C}$ is the input current, $\kappa = 2\pi/\lambda$ is the wavenumber, and λ is the wavelength. We next focus on an arbitrary user who is in the far field of the BS array. The user's location is described by the tuple $(r \cos \phi \sin \theta, r \sin \phi \sin \theta, r \cos \theta)$, where $r, \theta \in [0, \pi]$, and $\phi \in [0, 2\pi]$ are the radial distance, polar angle, and azimuth

¹We consider a linear array at the BS since it constitutes the building block of planar arrays. The planar case is investigated in Section VI-C and thereafter.

angle, respectively. The electric field at the user is then specified as (see Appendix A)

$$\mathbf{E}(r, \theta, \phi) = -j\eta \frac{e^{-j\kappa r}}{2\pi r} \sum_{n=0}^{N-1} e^{j\kappa \hat{\mathbf{r}} \cdot \mathbf{r}_n} I_n(0) \mathbf{F}(\theta, \phi), \quad (2)$$

where

$$\mathbf{F}(\theta, \phi) = \frac{\cos(\kappa\ell/2 \cos \phi \sin \theta) - \cos(\kappa\ell/2)}{\sin(\kappa\ell/2)(\sin^2 \phi + \cos^2 \phi \cos^2 \theta)} \times (\cos \theta \cos \phi \mathbf{e}_\theta - \sin \phi \mathbf{e}_\phi), \quad (3)$$

is the vector field pattern of each dipole, \mathbf{e}_θ and \mathbf{e}_ϕ are the unit vectors along the polar and azimuth directions, respectively, η is the characteristic impedance of free-space, $\hat{\mathbf{r}} = (\cos \phi \sin \theta, \sin \phi \sin \theta, \cos \theta)^T$ is the unit radial vector along the user direction, and $\mathbf{r}_n = (0, 0, nd)$ is the position vector of the n th antenna. The radiation intensity [W/sr] is written in vector form as

$$U \triangleq \frac{\|\mathbf{E}(r, \theta, \phi)\|^2}{2\eta} r^2 = \frac{\eta}{8\pi^2} \|\mathbf{F}(\theta, \phi)\|^2 |\mathbf{a}^H(\theta) \mathbf{i}|^2, \quad (4)$$

where $\mathbf{a}(\theta) = [e^{-j\kappa \hat{\mathbf{r}} \cdot \mathbf{r}_0}, \dots, e^{-j\kappa \hat{\mathbf{r}} \cdot \mathbf{r}_{N-1}}]^T \in \mathbb{C}^{N \times 1}$ and $\mathbf{i} = [I_0(0), \dots, I_{N-1}(0)]^T \in \mathbb{C}^{N \times 1}$ are the far-field array response vector and the vector of input currents, respectively. Using (4), the power radiated by the antenna array is

$$\begin{aligned} P_{\text{rad}} &= \int_0^{2\pi} \int_0^\pi U \sin \theta d\theta d\phi \\ &= \frac{1}{2} \mathbf{i}^H \underbrace{\left(\frac{\eta}{4\pi^2} \int_0^{2\pi} \int_0^\pi \mathbf{a}(\theta) \mathbf{a}^H(\theta) \|\mathbf{F}(\theta, \phi)\|^2 \sin \theta d\theta d\phi \right)}_{\text{Re}\{\mathbf{Z}_{\text{ideal}}\}} \mathbf{i} \\ &= \frac{1}{2} \mathbf{i}^H \text{Re}\{\mathbf{Z}_{\text{ideal}}\} \mathbf{i}, \end{aligned} \quad (5)$$

where $\mathbf{Z}_{\text{ideal}} \in \mathbb{C}^{N \times N}$ is the input impedance matrix of the array assuming *lossless* antennas. Moreover, $R_i \triangleq [\text{Re}\{\mathbf{Z}_{\text{ideal}}\}]_{n,n} = \frac{\eta}{4\pi^2} \int_0^{2\pi} \int_0^\pi \|\mathbf{F}(\theta, \phi)\|^2 \sin \theta d\theta d\phi$ is the input resistance² of each lossless dipole.

B. Input Power and Array Gain

Realistic dipole antennas exhibit a conduction/loss resistance which leads to heat dissipation. Because of the *skin effect* of conductive wires carrying an alternating current, the loss resistance per unit length is given by [26, Eq. (2-90b)]

$$\bar{R}_{\text{loss}} = \frac{1}{2\rho} \sqrt{\frac{\mu f}{\pi \sigma_c}}, \quad (6)$$

where f is the carrier frequency, μ is the permeability of free-space, and σ_c is the conductivity of the wire material. Under the sinusoidal current distribution in (1), the loss resistance relative to the input current $I_n(0)$ is then specified as

$$R_{\text{loss}} = \bar{R}_{\text{loss}} \int_{-\ell/2}^{\ell/2} \left| \frac{I_n(x')}{I_n(0)} \right|^2 dx' = \frac{\kappa\ell - \sin(\kappa\ell)}{4\kappa\rho \sin^2(\kappa\ell/2)} \sqrt{\frac{\mu f}{\pi \sigma_c}}, \quad (7)$$

²Recall that the input resistance equals the radiation resistance divided by $\sin^2(\kappa\ell/2)$ [26, Ch. 8]. This is because all quantities are expressed in terms of the input currents rather than the current maxima $\{I_n(0)/\sin(\kappa\ell/2)\}_{n=0}^{N-1}$.

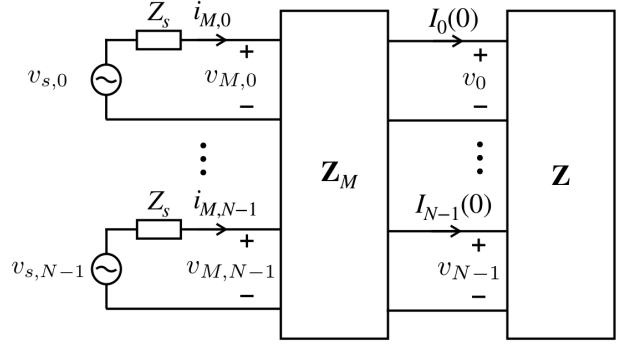


Fig. 2: Equivalent multi-port network of an antenna array covering signal generation, impedance matching, and mutual coupling.

which yields the overall power loss [27]

$$P_{\text{loss}} = \frac{1}{2} \sum_{n=0}^{N-1} R_{\text{loss}} |I_n(0)|^2 = \frac{1}{2} R_{\text{loss}} \|\mathbf{i}\|^2. \quad (8)$$

Consequently, the input power at the antenna ports is

$$\begin{aligned} P_{\text{in}} &= P_{\text{loss}} + P_{\text{rad}} \\ &= \frac{1}{2} R_{\text{loss}} \|\mathbf{i}\|^2 + \frac{1}{2} \mathbf{i}^H \text{Re}\{\mathbf{Z}_{\text{ideal}}\} \mathbf{i} = \frac{1}{2} \mathbf{i}^H \text{Re}\{\mathbf{Z}\} \mathbf{i}, \end{aligned} \quad (9)$$

where $\mathbf{Z} \triangleq R_{\text{loss}} \mathbf{I}_N + \mathbf{Z}_{\text{ideal}}$ is the impedance matrix of the lossy array. Finally, the array gain is defined as

$$G(\theta, \phi) \triangleq \frac{4\pi U}{P_{\text{in}}} = G_e(\theta, \phi) (R_{\text{loss}} + R_i) \frac{|\mathbf{a}^H(\theta) \mathbf{i}|^2}{\mathbf{i}^H \text{Re}\{\mathbf{Z}\} \mathbf{i}}, \quad (10)$$

where $G_e(\theta, \phi) = \frac{\eta \|\mathbf{F}(\theta, \phi)\|^2}{\pi (R_{\text{loss}} + R_i)}$ denotes the gain of each dipole.

C. Optimal Currents under Fixed Input Power

According to Friis transmission formula, the power received by the user is given by [26]

$$P_r = P_{\text{in}} \left(\frac{\lambda}{4\pi r} \right)^2 G(\theta, \phi), \quad (11)$$

where an isotropic antenna has been assumed at the user for simplicity. We now seek to find \mathbf{i} that maximizes the received power (or equivalently $G(\theta, \phi)$) subject to the input power constraint $P_{\text{in}} \leq P_t$. The objective (10) is a generalized Rayleigh quotient. Thus, the optimal current excitation is obtained as [27]

$$\mathbf{i}^{\text{opt}} = \sqrt{\frac{2P_t}{\mathbf{a}^H(\theta) \text{Re}\{\mathbf{Z}\}^{-1} \mathbf{a}(\theta)}} \text{Re}\{\mathbf{Z}\}^{-1} \mathbf{a}(\theta), \quad (12)$$

and the maximum array gain is

$$G_{\text{max}}(\theta, \phi) = G_e(\theta, \phi) (R_{\text{loss}} + R_i) \mathbf{a}^H(\theta) \text{Re}\{\mathbf{Z}\}^{-1} \mathbf{a}(\theta). \quad (13)$$

Remark 1 (Uncoupled ULA). *In the absence of mutual coupling, $\text{Re}\{\mathbf{Z}_{\text{ideal}}\} = R_i \mathbf{I}_N$ and $P_{\text{rad}} = \frac{1}{2} R_i \|\mathbf{i}\|^2$. Moreover, $\mathbf{i}^{\text{opt}} = \sqrt{\frac{2P_t}{N(R_{\text{loss}} + R_i)}} \mathbf{a}(\theta)$ and $G_{\text{max}}(\theta, \phi) = G_e(\theta, \phi) N$, which is the typical $O(N)$ power gain.*

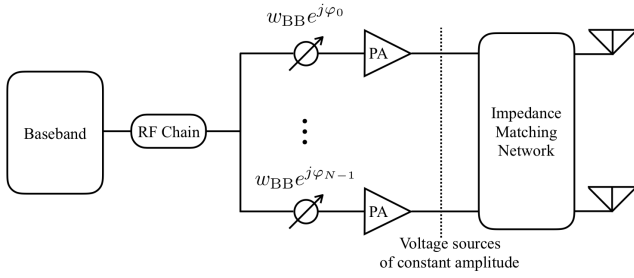


Fig. 3: Block diagram of hybrid array architecture with one RF chain.

III. IMPEDANCE MATCHING IN THE PRESENCE OF MUTUAL COUPLING

Mutual coupling alters the input impedance of each dipole. To see this, let $\mathbf{v} = [v_0, \dots, v_{N-1}]^T \in \mathbb{C}^{N \times 1}$ denote the vector of voltages at the antenna ports. Then, we have that $\mathbf{v} = \mathbf{Z}\mathbf{i} = \mathbf{Z}_a\mathbf{i}$, where $\mathbf{Z}_a \in \mathbb{C}^{N \times N}$ is a diagonal matrix with entries [26, Ch. 8]

$$[\mathbf{Z}_a]_{n,n} \triangleq \left([\mathbf{Z}]_{n,n} + \sum_{m=0, m \neq n}^{N-1} [\mathbf{Z}]_{n,m} \frac{I_m(0)}{I_n(0)} \right), \quad (14)$$

where $[\mathbf{Z}_a]_{n,n}$ is the *active* impedance of the n th antenna. The active impedance of each dipole hinges on the excitation currents, and hence single-port conjugate matching is optimal only for a specific beamforming angle θ [28]. For this reason, we resort to multi-port matching and model the BS array as in Fig. 2. The impedance network is a passive and *lossless* $2N$ -port network described by the matrix $\mathbf{Z}_M \in \mathbb{C}^{2N \times 2N}$, which is partitioned as

$$\mathbf{Z}_M = \begin{bmatrix} \mathbf{Z}_{M11} & \mathbf{Z}_{M12} \\ \mathbf{Z}_{M21} & \mathbf{Z}_{M22} \end{bmatrix}. \quad (15)$$

The lossless property implies that \mathbf{Z}_M has only imaginary entries. The vector of voltage sources is denoted by $\mathbf{v}_s = [v_{s,0}, \dots, v_{s,N-1}]^T \in \mathbb{C}^{N \times 1}$. Each voltage source has an internal impedance $Z_s \in \mathbb{C}$, with $\text{Re}\{Z_s\} = R_s$. Likewise, the voltages and currents at the input ports of the network are denoted by $\mathbf{v}_M = [v_{M,0}, \dots, v_{M,N-1}]^T \in \mathbb{C}^{N \times 1}$ and $\mathbf{i}_M = [i_{M,0}, \dots, i_{M,N-1}]^T \in \mathbb{C}^{N \times 1}$, respectively. Based on basic circuit analysis, the relationship between the voltages and currents at the input and output of the matching network is [29]

$$\begin{bmatrix} \mathbf{v}_M \\ \mathbf{v} \end{bmatrix} = \begin{bmatrix} \mathbf{Z}_{M11} & \mathbf{Z}_{M12} \\ \mathbf{Z}_{M21} & \mathbf{Z}_{M22} \end{bmatrix} \begin{bmatrix} \mathbf{i}_M \\ -\mathbf{i} \end{bmatrix}. \quad (16)$$

Using (16) and the relationship $\mathbf{v} = \mathbf{Z}\mathbf{i}$ yields

$$\mathbf{v}_M = \underbrace{(\mathbf{Z}_{M11} - \mathbf{Z}_{M12}(\mathbf{Z} + \mathbf{Z}_{M22})^{-1}\mathbf{Z}_{M21})}_{\mathbf{Z}_T} \mathbf{i}_M, \quad (17)$$

where $\mathbf{Z}_T \in \mathbb{C}^{N \times N}$ is the overall transmit impedance matrix accounting for power matching and mutual coupling. The problem of optimal multi-port matching is to find \mathbf{Z}_M so that $\mathbf{Z}_T = Z_s^* \mathbf{I}_N$. In this case, there are no reflection losses and half of the generated power enters the antenna array, i.e.,

maximum power transfer [30]. This is accomplished for [29]

$$\mathbf{Z}_M = \begin{bmatrix} -j\text{Im}\{Z_s\}\mathbf{I}_N & -j\sqrt{R_s}\text{Re}\{\mathbf{Z}\}^{1/2} \\ -j\sqrt{R_s}\text{Re}\{\mathbf{Z}\}^{1/2} & -j\text{Im}\{\mathbf{Z}\} \end{bmatrix}. \quad (18)$$

Under (18), we have that

$$\mathbf{v}_s = Z_s \mathbf{I}_N \mathbf{i}_M + \mathbf{v}_M = (Z_s \mathbf{I}_N + \mathbf{Z}_T) \mathbf{i}_M = 2R_s \mathbf{i}_M, \quad (19)$$

and the total power generated by the voltage sources is

$$P_{\text{total}} = \frac{1}{2} \text{Re}\{\mathbf{v}_s^H \mathbf{i}_M\} = R_s \|\mathbf{i}_M\|^2. \quad (20)$$

From (16) and (18), it also holds that

$$\begin{aligned} \mathbf{i}_M &= \mathbf{Z}_{M21}^{-1} (\mathbf{Z} + \mathbf{Z}_{M22}) \mathbf{i} \\ &= \frac{j}{\sqrt{R_s}} \text{Re}\{\mathbf{Z}\}^{1/2} \mathbf{i}, \end{aligned} \quad (21)$$

and hence $P_{\text{total}} = \mathbf{i}^H \text{Re}\{\mathbf{Z}\} \mathbf{i} = 2P_{\text{in}}$, which confirms the optimality of (18).

IV. HARDWARE-EFFICIENT IMPLEMENTATION OF SUPERDIRECTIONAL BEAMSTEERING

In this section, we investigate the problem of generating a superdirective beam with a single RF chain and a low-complexity impedance matching network.

A. Problem Statement

From (12), (19), and (21), the vector of voltage sources maximizing the array gain is given by

$$\begin{aligned} \mathbf{v}_s^{\text{opt}} &= 2R_s \mathbf{i}_M^{\text{opt}} = j2\sqrt{R_s} \text{Re}\{\mathbf{Z}\}^{1/2} \mathbf{i}^{\text{opt}} \\ &= j2\sqrt{\frac{2R_s P_t}{\mathbf{a}^H(\theta) \text{Re}\{\mathbf{Z}\}^{-1} \mathbf{a}(\theta)}} \text{Re}\{\mathbf{Z}\}^{-1/2} \mathbf{a}(\theta). \end{aligned} \quad (22)$$

In most massive MIMO studies, beamforming is conveniently described by a complex vector $\mathbf{w} \in \mathbb{C}^{N \times 1}$ whose squared norm, $\|\mathbf{w}\|^2$, defines the transmit power. This representation originates from information theory and can be mapped to the voltage sources driving the array through the relationship [31]

$$\begin{aligned} \mathbf{w} &= -\frac{1}{j2\sqrt{R_s}} (\mathbf{v}_s^{\text{opt}})^* \\ &= \sqrt{\frac{2P_t}{\mathbf{a}^H(\theta) \text{Re}\{\mathbf{Z}\}^{-1} \mathbf{a}(\theta)}} \text{Re}\{\mathbf{Z}\}^{-1/2} \mathbf{a}^*(\theta). \end{aligned} \quad (23)$$

We next consider a hybrid analog-digital array with one RF chain and N analog phase shifters, as shown in Fig. 3. In this case, $\mathbf{w} = w_{\text{BB}} [e^{j\varphi_0}, \dots, e^{j\varphi_{N-1}}]^T$, where w_{BB} denotes the complex amplitude of baseband processing whilst $\{\varphi_n\}_{n=0}^{N-1}$ are the variable phases. Consequently, beamsteering requires voltage sources $\{v_{s,n}\}_{n=0}^{N-1}$ of uniform magnitude. From (22), it is easy to verify that $\mathbf{v}_s^{\text{opt}}$ has entries of different magnitudes, and hence cannot be realized by a single RF chain. In summary, superdirective ULAs require amplitude control at each antenna, which can be provided by a fully digital array or an active phased array with digitally controlled amplitude attenuators. However, those architectures increase substantially the hardware complexity and power consumption.

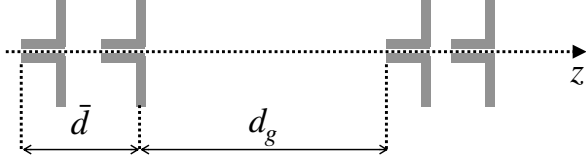


Fig. 4: Example of a NULA with $N_g = \bar{N} = 2$.

Similarly, multi-port matching requires interconnections and circuit components between all the $2N$ ports [32]. Thus, it is prohibitively complex for a large number N of antennas [33].

B. Proposed Solution

1) *Nonuniform Linear Array*: The BS array is divided into N_g groups of \bar{N} antennas each, i.e., $N = N_g \bar{N}$. Let d_g and \bar{d} denote the inter-group and inter-element spacings, respectively, as shown in Fig. 4. The distance of the \bar{n} th element in the n_g th subarray from the origin of the coordinate system is given by $(\bar{n}\bar{d} + n_g(d_g + (\bar{N} - 1)\bar{d})) \cos \theta$, where $\bar{n} = 0, \dots, \bar{N} - 1$ and $n_g = 0, \dots, N_g - 1$. Thus, the array response vector $\mathbf{a}(\theta)$ can be recast as

$$\begin{aligned} \mathbf{a}(\theta) &= \left[\mathbf{a}_0(\theta), \mathbf{a}_0(\theta)e^{-j\kappa((d_g + (\bar{N}-1)\bar{d}) \cos \theta)}, \dots, \right. \\ &\quad \left. \mathbf{a}_0(\theta)e^{-j\kappa(N_g-1)(d_g + (\bar{N}-1)\bar{d}) \cos \theta} \right]^T \\ &= \mathbf{a}_g(\theta) \otimes \mathbf{a}_0(\theta), \end{aligned} \quad (24)$$

where $\mathbf{a}_0(\theta) \triangleq [1, \dots, e^{-j\kappa(\bar{N}-1)\bar{d} \cos \theta}]^T \in \mathbb{C}^{\bar{N} \times 1}$ is the response vector of the 0th antenna group, and $\mathbf{a}_g(\theta) \triangleq [1, \dots, e^{-j\kappa(N_g-1)(d_g + (\bar{N}-1)\bar{d}) \cos \theta}]^T \in \mathbb{C}^{N_g \times 1}$ is the response vector between groups. Similarly, the input impedance matrix is partitioned as

$$\mathbf{Z} = \begin{bmatrix} \mathbf{Z}_0 & \mathbf{Z}_{0,1} & \cdots & \mathbf{Z}_{0,N_g-1} \\ \mathbf{Z}_{1,0} & \mathbf{Z}_0 & \cdots & \mathbf{Z}_{1,N_g-1} \\ \vdots & \vdots & \ddots & \vdots \\ \mathbf{Z}_{N_g-1,0} & \mathbf{Z}_{N_g-1,1} & \cdots & \mathbf{Z}_0 \end{bmatrix}, \quad (25)$$

where $\text{Re}\{\mathbf{Z}_{n_{g1}, n_{g2}}\} \in \mathbb{R}^{\bar{N} \times \bar{N}}$ and $\text{Re}\{\mathbf{Z}_0\} \in \mathbb{R}^{\bar{N} \times \bar{N}}$ are defined by (26) and (27) at the bottom of this page, respectively. In fact, \mathbf{Z}_0 corresponds to the input impedance matrix of each \bar{N} -element group. For $\bar{N} = 2$, we have

$$\text{Re}\{\mathbf{Z}_0\} \triangleq \begin{bmatrix} R_{\text{self}} & R_m \\ R_m & R_{\text{self}} \end{bmatrix}, \quad (28)$$

where $R_{\text{self}} = R_{\text{loss}} + R_i$ denotes the self impedance for notational convenience, and R_m is the real part of the mutual impedance between two adjacent dipoles.

When the inter-group spacing is sufficiently large, the coupling between groups can be neglected. Thus, $\text{Re}\{\mathbf{Z}_{n_{g1}, n_{g2}}\} \approx \mathbf{0}_{\bar{N} \times \bar{N}}$ for $n_{g1} \neq n_{g2}$, which makes \mathbf{Z} approximately a block diagonal matrix, namely $\text{Re}\{\mathbf{Z}\} \approx \mathbf{I}_{N_g} \otimes \text{Re}\{\mathbf{Z}_0\} = \text{Re}\{\mathbf{Z}_{\text{approx}}\}$. We finally stress that in addition to a large d_g , the mutual coupling between antenna groups can be further reduced through various decoupling techniques, such as electromagnetic band gap structures placed between them [34].

2) *Coupled Antenna Pairs*: A major drawback of beamsteering under mutual coupling is the requirement of amplitude control at each voltage source. However, in a NULA, all antenna groups share the same voltage amplitudes. This is because from (22)

$$\begin{aligned} \mathbf{v}_s^{\text{opt}} &= \bar{v} \text{Re}\{\mathbf{Z}\}^{-1/2} \mathbf{a}(\theta) \\ &\approx \bar{v} \text{Re}\{\mathbf{Z}_{\text{approx}}\}^{-1/2} \mathbf{a}(\theta) \\ &= \bar{v} \left(\mathbf{I}_{N_g} \otimes \text{Re}\{\mathbf{Z}_0\}^{-1/2} \right) (\mathbf{a}_g(\theta) \otimes \mathbf{a}_0(\theta)) \\ &= \bar{v} \mathbf{a}_g(\theta) \otimes \left(\text{Re}\{\mathbf{Z}_0\}^{-1/2} \mathbf{a}_0(\theta) \right), \end{aligned} \quad (29)$$

where $\bar{v} = j2\sqrt{2R_s P_t / \mathbf{a}^H(\theta) \text{Re}\{\mathbf{Z}\}^{-1} \mathbf{a}(\theta)}$, which gives

$$\text{mag}(\mathbf{v}_s^{\text{opt}}) = \bar{v} \begin{bmatrix} \text{mag}(\text{Re}\{\mathbf{Z}_0\}^{-1/2} \mathbf{a}_0(\theta)) \\ \vdots \\ \text{mag}(\text{Re}\{\mathbf{Z}_0\}^{-1/2} \mathbf{a}_0(\theta)) \end{bmatrix}. \quad (30)$$

By leveraging this unique property of NULAs, we further propose two-element groups. The following proposition justifies the choice of $\bar{N} = 2$.

Proposition 1. For $\bar{N} = 2$, $\text{mag}(\text{Re}\{\mathbf{Z}_0\}^{-1/2} \mathbf{a}_0(\theta))$ reduces to (31) at the top of the next page.

Proof. See Appendix B. \square

According to Proposition 1, antenna pairs result in *uniform* excitation amplitudes $\{v_{s,n}\}_{n=0}^{\bar{N}-1}$, thereby enabling the realization of superdirective beamsteering with a single RF chain and N analog phase shifters. Additionally, each antenna pair is separately matched using the four-port network (see Appendix B)

$$\mathbf{Z}_{M,0} = \begin{bmatrix} -j\text{Im}\{Z_s\} \mathbf{I}_2 & -j\sqrt{R_s} \text{Re}\{\mathbf{Z}_0\}^{1/2} \\ -j\sqrt{R_s} \text{Re}\{\mathbf{Z}_0\}^{1/2} & -j\text{Im}\{\mathbf{Z}_0\} \end{bmatrix}. \quad (32)$$

Therefore, the proposed solution also facilitates the implementation of optimal multi-port matching, which would not be feasible in a coupled ULA with a large number of elements. Note that our solution relies on the symmetric structure of $\mathbf{Z}_0 \in \mathbb{C}^{2 \times 2}$, which holds for radiators beyond linear dipoles. The main reason we chose dipoles is mathematical tractability; otherwise, we would heavily rely on full-wave simulations to assess the antenna array gain. The problem of finding the

$$\text{Re}\{\mathbf{Z}_{n_{g1}, n_{g2}}\} \triangleq \frac{\eta}{4\pi^2} \int_0^{2\pi} \int_0^\pi \mathbf{a}_0(\theta) \mathbf{a}_0^H(\theta) e^{-j\kappa(n_{g1} - n_{g2})(d_g + (\bar{N}-1)\bar{d}) \cos \theta} \|\mathbf{F}(\theta, \phi)\|^2 \sin \theta d\theta d\phi, \quad \text{for } n_{g1} \neq n_{g2}, \quad (26)$$

$$\text{Re}\{\mathbf{Z}_0\} \triangleq \text{Re}\{\mathbf{Z}_{n_{g1}, n_{g2}}\} = \frac{\eta}{4\pi^2} \int_0^{2\pi} \int_0^\pi \mathbf{a}_0(\theta) \mathbf{a}_0^H(\theta) \|\mathbf{F}(\theta, \phi)\|^2 \sin \theta d\theta d\phi + R_{\text{loss}} \mathbf{I}_{\bar{N}}, \quad \text{for } n_{g1} = n_{g2}. \quad (27)$$

$$\begin{aligned} \text{mag} \left(\text{Re} \{ \mathbf{Z}_0 \}^{-1/2} \mathbf{a}_0(\theta) \right) &= \mathbf{1}_{2 \times 1} \frac{1}{\sqrt{2R_{\text{self}} + 2\sqrt{R_{\text{self}}^2 - R_m^2}}} \\ &\times \sqrt{\left(\frac{R_{\text{self}}}{\sqrt{R_{\text{self}}^2 - R_m^2}} + 1 \right)^2 + \frac{R_m^2}{R_{\text{self}}^2 - R_m^2} - 2 \left(\frac{R_{\text{self}}}{\sqrt{R_{\text{self}}^2 - R_m^2}} + 1 \right) \frac{R_m}{\sqrt{R_{\text{self}}^2 - R_m^2}} \cos(\kappa \bar{d} \cos \theta)}. \end{aligned} \quad (31)$$

optimal antenna type to facilitate superdirectivity is beyond the scope of the current work, and is a promising avenue for future research.

V. THZ MASSIVE MIMO MODEL

In this section, we introduce the high-level system model used to evaluate the performance of the proposed NULA in terms of the achievable rate and EE.

A. Signal Model

Consider a THz massive MIMO system, where the BS serves $K \ll N$ single-antenna users. Let $\mathbf{h}_k \in \mathbb{C}^{N \times 1}$ and β_k denote the small-scale fading channel and path loss of user k , respectively. The downlink channel of user k is then specified as $\sqrt{\beta_k} \mathbf{h}_k^T$. To facilitate hardware implementation, a fully connected analog-digital array with N_{RF} RF chains is considered at the BS [35]. Thus, the precoder is decomposed as $\mathbf{W} = \mathbf{W}_{\text{RF}} \mathbf{W}_{\text{BB}} = [\mathbf{w}_1, \dots, \mathbf{w}_{N_{\text{RF}}}] \in \mathbb{C}^{N \times N_{\text{RF}}}$, where $\mathbf{W}_{\text{RF}} \in \mathbb{C}^{N \times N_{\text{RF}}}$ is the RF beamformer realized by analog phase shifters, whereas $\mathbf{W}_{\text{BB}} \in \mathbb{C}^{N_{\text{RF}} \times N_{\text{RF}}}$ is the baseband precoder. Without loss of generality, we assume $N_{\text{RF}} = K$ hereafter. Let $\mathbf{x} = [x_1, \dots, x_K]^T \sim \mathcal{CN}(\mathbf{0}_{K \times 1}, \mathbf{I}_K)$ be the vector of users' data symbols. The transmitted signal is then given by $\mathbf{W}\mathbf{x} \in \mathbb{C}^{N \times 1}$, and should satisfy the power constraint

$$\mathbb{E} \{ \|\mathbf{W}\mathbf{x}\|^2 \} = \sum_{k=1}^K \|\mathbf{w}_k\|^2 \leq 2P_t, \quad (33)$$

where $2P_t$ is the *total power* under perfect impedance matching. Given the above, the received baseband signal at the k th user is written as

$$y_k = \sqrt{\beta_k} \mathbf{h}_k^T \mathbf{w}_k x_k + \sqrt{\beta_k} \sum_{i=1, i \neq k}^K \mathbf{h}_k^T \mathbf{w}_i x_i + n_k, \quad (34)$$

where $n_k \sim \mathcal{CN}(0, \sigma^2)$ is the additive noise. Finally, the signal-to-interference-plus-noise ratio (SINR) of user k is

$$\text{SINR}_k = \frac{\beta_k |\mathbf{h}_k^T \mathbf{w}_k|^2}{\beta_k \sum_{i=1, i \neq k}^K |\mathbf{h}_k^T \mathbf{w}_i|^2 + B\sigma^2}, \quad (35)$$

where $B\sigma^2$ is the noise power over the transmit bandwidth B .

B. Channel Model

Because of the severe path attenuation in the THz band, multi-path scattering is very limited. We therefore assume line-of-sight (LoS) links between the BS and users, akin to [36]. In

the presence of mutual coupling at the BS array, the channel vector of user k is expressed as [29, Eq. (105)]

$$\mathbf{h}_k \triangleq \text{Re} \{ \bar{\mathbf{Z}} \}^{-1/2} \mathbf{a}(\theta_k), \quad (36)$$

where $\bar{\mathbf{Z}} \triangleq \frac{1}{R_{\text{loss}} + R_t} \mathbf{Z}$ is the *normalized* input impedance matrix of the BS array.³ Finally, because the molecular absorption losses are no longer negligible at THz frequencies, the path loss coefficient is calculated as [37]

$$\beta_k = G_e(\theta_k, \phi_k) \left(\frac{\lambda}{4\pi r_k} \right)^2 e^{-\kappa_{\text{abs}} r_k}, \quad (37)$$

where $G_e(\theta_k, \phi_k)$ is the gain of each BS antenna, λ is the carrier wavelength, r_k is the distance from the BS to user k , and κ_{abs} is the molecular absorption coefficient determined by the composition of the propagation medium [38].

C. Power Consumption Model

For a fully-connected array structure, the overall power consumption is given by [39]

$$P_c = P_{\text{BB}} + KP_{\text{RF}} + KN P_{\text{PS}} + NP_{\text{PA}} + P_t + P_{\text{CE}}, \quad (38)$$

where P_{BB} , P_{RF} , P_{PS} , P_{PA} , and P_{CE} denote the powers consumed by a baseband unit, an RF chain, a phase shifter, a power amplifier, and the channel estimation process, respectively. Moreover, each RF chain comprises a digital-to-analog converter (DAC), a local oscillator, and a mixer, and hence $P_{\text{RF}} = P_{\text{DAC}} + P_{\text{LO}} + P_{\text{M}}$. We finally stress that the power consumption of splitters and combiners is negligible, and hence is ignored [39].

VI. SIGNAL AND INTERFERENCE POWERS

A. Proposed NULA

We consider MRT at the BS. Under equal power allocation, we have that

$$\begin{aligned} \mathbf{w}_k &= \sqrt{\frac{2P_t}{K}} \frac{\mathbf{h}_k^*}{\|\mathbf{h}_k\|} \\ &= \sqrt{\frac{2P_t}{K \mathbf{a}^H(\theta_k) \text{Re} \{ \bar{\mathbf{Z}} \}^{-1} \mathbf{a}(\theta_k)}} \text{Re} \{ \bar{\mathbf{Z}} \}^{-\frac{1}{2}} \mathbf{a}^*(\theta_k), \end{aligned} \quad (39)$$

and the power of the desired signal, normalized by $K/(2P_t)$, is

$$\frac{K}{2P_t} |\mathbf{h}_k^T \mathbf{w}_k|^2 = \mathbf{a}^H(\theta_k) \text{Re} \{ \bar{\mathbf{Z}} \}^{-1} \mathbf{a}(\theta_k). \quad (40)$$

³The normalized input impedance matrix is used for notational convenience. In this way, the array gain is recast as $G(\theta, \phi) = G_e(\theta, \phi) \frac{|\mathbf{a}^H(\theta) \mathbf{i}|^2}{\text{Re} \{ \bar{\mathbf{Z}} \}^{-1}}$, and the path loss coefficient or channel vector will not include the term $R_{\text{loss}} + R_t$. For example, $\text{Re} \{ \bar{\mathbf{Z}} \} = \mathbf{I}_N$ and $\mathbf{h}_k = \mathbf{a}(\theta_k)$ in the absence of coupling.

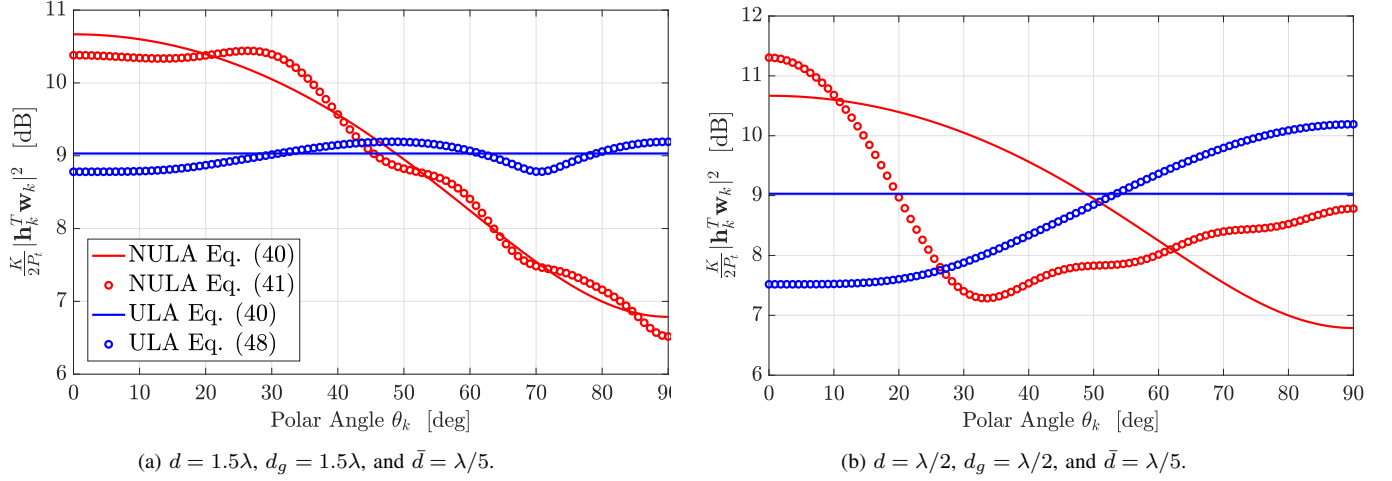


Fig. 5: Normalized signal power versus polar angle for $N = 8$ dipoles of $\ell = \lambda/2$, $\rho = \lambda/500$, and $\sigma_c = 5.7 \times 10^7$ S/m. In NULA, $\bar{N} = 2$ and $N_g = 4$. The carrier frequency is set to $f = 300$ GHz.

Due to the block-diagonal structure of $\bar{\mathbf{Z}}$, (40) simplifies to by

$$\begin{aligned} \frac{K}{2P_t} |\mathbf{h}_k^T \mathbf{w}_k|^2 &\approx \mathbf{a}^H(\theta_k) \text{Re} \{ \bar{\mathbf{Z}}_{\text{approx}} \}^{-1} \mathbf{a}(\theta_k) \\ &= (\mathbf{a}_g^H(\theta_k) \otimes \mathbf{a}_0^H(\theta_k)) (\mathbf{I}_{N_g} \otimes \text{Re} \{ \bar{\mathbf{Z}}_0 \}^{-1}) (\mathbf{a}_g(\theta_k) \otimes \mathbf{a}_0(\theta_k)) \\ &= N_g \mathbf{a}_0^H(\theta_k) \text{Re} \{ \bar{\mathbf{Z}}_0 \}^{-1} \mathbf{a}_0(\theta_k), \end{aligned} \quad (41)$$

where $\bar{\mathbf{Z}}_{\text{approx}} = \frac{1}{R_{\text{loss}} + R_i} \mathbf{Z}_{\text{approx}}$ and $\bar{\mathbf{Z}}_0 = \frac{1}{R_{\text{loss}} + R_i} \mathbf{Z}_0$. As seen from (41), the power gain of the NULA is N_g times the gain of a superdirective antenna group. In the sequel, we determine $\mathbf{a}_0^H(\theta_k) \text{Re} \{ \bar{\mathbf{Z}}_0 \}^{-1} \mathbf{a}_0(\theta_k)$ in closed-form for $\bar{N} = 2$. We first have that

$$\text{Re} \{ \bar{\mathbf{Z}}_0 \} = \begin{bmatrix} 1 & \bar{R}_m \\ \bar{R}_m & 1 \end{bmatrix}, \quad (42)$$

where $\bar{R}_m = \frac{1}{R_{\text{loss}} + R_i} R_m$. Then, the inverse matrix is determined as

$$\text{Re} \{ \bar{\mathbf{Z}}_0 \}^{-1} = \frac{1}{1 - \bar{R}_m^2} \begin{bmatrix} 1 & -\bar{R}_m \\ -\bar{R}_m & 1 \end{bmatrix}, \quad (43)$$

and

$$\begin{aligned} \text{Re} \{ \bar{\mathbf{Z}}_0 \}^{-1} \mathbf{a}_0(\theta_k) &= \frac{1}{1 - \bar{R}_m^2} \begin{bmatrix} 1 & -\bar{R}_m \\ -\bar{R}_m & 1 \end{bmatrix} \begin{bmatrix} 1 \\ e^{-j\kappa \bar{d} \cos \theta_k} \end{bmatrix} \\ &= \frac{1}{1 - \bar{R}_m^2} \begin{bmatrix} 1 - \bar{R}_m e^{-j\kappa \bar{d} \cos \theta_k} \\ -\bar{R}_m + e^{-j\kappa \bar{d} \cos \theta_k} \end{bmatrix}, \end{aligned} \quad (44)$$

which gives

$$\begin{aligned} \mathbf{a}_0^H(\theta_k) \text{Re} \{ \bar{\mathbf{Z}}_0 \}^{-1} \mathbf{a}_0(\theta_k) &= \frac{1}{1 - \bar{R}_m^2} \left(1 - \bar{R}_m e^{-j\kappa \bar{d} \cos \theta_k} - \bar{R}_m e^{j\kappa \bar{d} \cos \theta_k} + 1 \right) \\ &= \frac{2}{1 - \bar{R}_m^2} \left(1 - \bar{R}_m \cos(\kappa \bar{d} \cos \theta_k) \right). \end{aligned} \quad (45)$$

According to (45), $\mathbf{a}_0^H(\theta_k) \text{Re} \{ \bar{\mathbf{Z}}_0 \}^{-1} \mathbf{a}_0(\theta_k) \approx 2$ for large \bar{d} , i.e., $\bar{R}_m \approx 0$, which corresponds to the conventional power gain of a two-element array.

In a similar manner, the interference power at user k from the beam toward user $i \neq k$, normalized by $K/(2P_t)$, is given

$$\begin{aligned} \frac{K}{2P_t} |\mathbf{h}_k^T \mathbf{w}_i|^2 &= \frac{|\mathbf{a}^H(\theta_k) \text{Re} \{ \bar{\mathbf{Z}} \}^{-1} \mathbf{a}(\theta_i)|^2}{\mathbf{a}^H(\theta_i) \text{Re} \{ \bar{\mathbf{Z}} \}^{-1} \mathbf{a}(\theta_i)} \\ &\approx \frac{|\mathbf{a}^H(\theta_k) \text{Re} \{ \bar{\mathbf{Z}}_{\text{approx}} \}^{-1} \mathbf{a}(\theta_i)|^2}{\mathbf{a}^H(\theta_i) \text{Re} \{ \bar{\mathbf{Z}}_{\text{approx}} \}^{-1} \mathbf{a}(\theta_i)} \\ &\stackrel{(a)}{=} N_g |D_{N_g}(\kappa(d_g + (\bar{N} - 1)\bar{d})(\cos \theta_k - \cos \theta_i))|^2 \\ &\quad \times \frac{|\mathbf{a}_0^H(\theta_k) \text{Re} \{ \bar{\mathbf{Z}}_0 \}^{-1} \mathbf{a}_0(\theta_i)|^2}{\mathbf{a}_0^H(\theta_i) \text{Re} \{ \bar{\mathbf{Z}}_0 \}^{-1} \mathbf{a}_0(\theta_i)}, \end{aligned} \quad (46)$$

where (a) is proven in Appendix C. From (44) and (45), we finally have that

$$\begin{aligned} \frac{|\mathbf{a}_0^H(\theta_k) \text{Re} \{ \bar{\mathbf{Z}}_0 \}^{-1} \mathbf{a}_0(\theta_i)|^2}{\mathbf{a}_0^H(\theta_i) \text{Re} \{ \bar{\mathbf{Z}}_0 \}^{-1} \mathbf{a}_0(\theta_i)} &= \frac{|1 + e^{j\kappa \bar{d}(\cos \theta_k - \cos \theta_i)} - \bar{R}_m (e^{j\kappa \bar{d} \cos \theta_k} + e^{-j\kappa \bar{d} \cos \theta_i})|^2}{2(1 - \bar{R}_m^2)(1 - \bar{R}_m \cos(\kappa \bar{d} \cos \theta_i))}. \end{aligned} \quad (47)$$

B. Comparison With Uncoupled ULA

In the massive MIMO literature, it is customary to consider a uniform inter-element spacing [40]. Furthermore, mutual coupling is avoided by employing a sufficiently large d so that $\text{Re} \{ \bar{\mathbf{Z}} \} \approx \mathbf{I}_N$. In this case, the normalized power of the desired signal becomes

$$\frac{K}{2P_t} |\mathbf{h}_k^T \mathbf{w}_k|^2 \approx N, \quad (48)$$

whereas the normalized interference is

$$\frac{K}{2P_t} |\mathbf{h}_k^T \mathbf{w}_i|^2 \approx N |D_N(\kappa d(\cos \theta_k - \cos \theta_i))|^2. \quad (49)$$

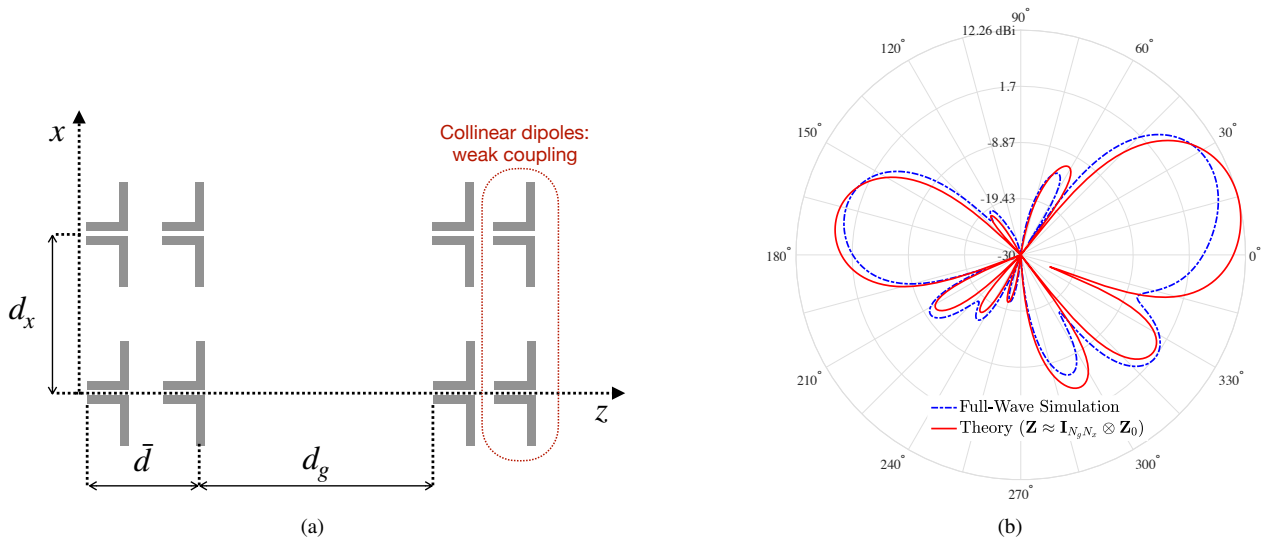


Fig. 6: (a) Example of a NUPA with $N_x = N_g = \bar{N} = 2$; and (b) theoretical beam pattern (52) against full-wave simulation for $d_x = 0.7\lambda$, $d_g = 1.5\lambda$, and $\bar{d} = \lambda/5$. The desired beamforming direction is $(\theta_i, \phi_i) = (20^\circ, 0^\circ)$.

From (48), it is evident that the power gain is independent of the steering direction θ_k in an uncoupled ULA. This assumption is safely made for a large antenna separation, as showcased in Fig. 5. Specifically, half-wavelength spacing does create coupling between directional antennas, and hence the input impedance matrix cannot be ignored.⁴ Lastly, according to the approximate expressions, the proposed NULA with $\bar{N} = 2$ yields a *relative* power gain equal to

$$\begin{aligned} & N_g \mathbf{a}_0^H(\theta_k) \text{Re} \{ \bar{\mathbf{Z}}_0 \}^{-1} \mathbf{a}_0(\theta_k) - N \\ &= N_g \left[\mathbf{a}_0^H(\theta_k) \text{Re} \{ \bar{\mathbf{Z}}_0 \}^{-1} \mathbf{a}_0(\theta_k) - 2 \right] = O(N_g), \end{aligned} \quad (50)$$

which scales linearly with N_g for some $\theta_k \in [0, \theta_{\max}]$; for example, $\theta_{\max} \approx 50^\circ$ in Fig. 5(a). This trade off between directivity and angular coverage is fundamental [42]. Thus, increasing the former inevitably decreases the latter, and vice versa. Whether it is beneficial to have a highly directive array depends on the propagation environment and deployment scenario [42], [43].

C. Extension to Planar Arrays

In this section, we extend the proposed design to planar arrays, which are of practical importance. Specifically, a NUPA is formed by placing N_x NULAs along the x -axis with inter-element spacing d_x , as depicted in Fig. 6(a). The total number of antennas is $N = N_x N_g \bar{N}$. Also, the response vector of the NUPA is given by $\mathbf{a}(\theta, \phi) = \mathbf{a}_x(\theta, \phi) \otimes \mathbf{a}_g(\theta) \otimes \mathbf{a}_0(\theta)$, where $\mathbf{a}_x(\theta, \phi) \triangleq [1, \dots, e^{-j\kappa(N_x-1)d_x \cos \phi \sin \theta}]^T \in \mathbb{C}^{N_x \times 1}$. The coupling between the NULAs is very small for $d_x \geq \lambda/2$ since adjacent dipoles along the x -axis are collinear. Given that, the impedance matrix of the NUPA reduces to $\mathbf{Z} \approx \mathbf{I}_{N_g N_x} \otimes \mathbf{Z}_0$, while the signal and interference powers in (40) and (46) are recast, respectively, as

$$\frac{K}{2P_t} |\mathbf{h}_k^T \mathbf{w}_k|^2 \approx N_x N_g \mathbf{a}_0^H(\theta_k) \text{Re} \{ \bar{\mathbf{Z}}_0 \}^{-1} \mathbf{a}_0(\theta_k), \quad (51)$$

⁴The assumption of uncoupled elements under half-wavelength spacing holds only for isotropic radiators [41].

and

$$\begin{aligned} & \frac{K}{2P_t} |\mathbf{h}_k^T \mathbf{w}_i|^2 \approx \\ & \approx N_x N_g |D_{N_x}(\kappa d_x (\cos \phi_k \sin \theta_k - \cos \phi_i \sin \theta_i))|^2 \\ & \times |D_{N_g}(d_g + (\bar{N} - 1)\bar{d})(\cos \theta_k - \cos \theta_i)|^2 \\ & \times \frac{|\mathbf{a}_0^H(\theta_k) \text{Re} \{ \bar{\mathbf{Z}}_0 \}^{-1} \mathbf{a}_0(\theta_i)|^2}{\mathbf{a}_0^H(\theta_i) \text{Re} \{ \bar{\mathbf{Z}}_0 \}^{-1} \mathbf{a}_0(\theta_i)}. \end{aligned} \quad (52)$$

From (51), we see that the signal power is N_x times that of a NULA with N_g dipole pairs, as expected. Regarding the interference power, NUPA offers an additional degree of freedom compared to a single NULA along the z -axis, which is given by the term $N_x |D_{N_x}(\kappa d_x (\cos \phi_k \sin \theta_k - \cos \phi_i \sin \theta_i))|^2$. The good accuracy of (52) is confirmed in Fig. 6(b) considering the polar plane $\phi_k = \phi_i = 0$. Note that the full-wave simulation was performed using the Antenna Toolbox of MATLAB.

VII. CHANNEL ESTIMATION

So far, we have assumed perfect channel knowledge at the BS and analyzed the performance of MRT in the presence of mutual coupling. In this section, we focus on the channel estimation problem, which is crucial to beamforming.

A. Channel Reciprocity

In massive MIMO, it is typical to invoke channel reciprocity for time-division duplex (TDD) operation [44]. This enables the BS to estimate the downlink channel through uplink pilots sent by users. Let $\mathbf{h}_{k,\text{DL}} = \mathbf{h}_k^T \in \mathbb{C}^{1 \times N}$ denote the downlink channel, where \mathbf{h}_k is given by (36). The TDD assumption is then that $\mathbf{h}_{k,\text{UL}} = \mathbf{h}_{k,\text{DL}}^T$. Although the physical channels (i.e., those defined by electromagnetic theory) are reciprocal, this does not generally hold for their information-theoretic counterparts in the presence of antenna mutual coupling [45].

In particular, the BS needs to employ a linear transformation to compute $\mathbf{h}_{k,\text{DL}}^T$ from the estimated $\mathbf{h}_{k,\text{UL}}$. Nevertheless, the transmit and receive array gains coincide with each other under isotropic background noise and noise matching at the receiver [29, Eq. (97)]. Thus, we can assume that $\mathbf{h}_{k,\text{UL}} = \mathbf{h}_{k,\text{DL}}^T$, and that the reception strategy maximizing the signal-to-noise ratio (SNR) of each user k is the maximum ratio combiner $\mathbf{v}_k = \mathbf{h}_k^H / \|\mathbf{h}_k\|$.

B. Problem Formulation

We assume a block-fading model, where the channel coherence time is much larger than the training period. The BS estimates the uplink channel \mathbf{h}_k of each user k in rounds. Subsequently, we focus on an arbitrary user and omit the subscript “ k ”. Specifically, the training period for each user consists of N_{slot} time slots. At each time slot $t = 1, \dots, N_{\text{slot}}$, the user transmits the pilot signal $x_t = \sqrt{P_p}$, where P_p is the power per pilot signal. In turn, the BS combines the received pilot signal using a training hybrid combiner $\mathbf{V}_t = \mathbf{V}_{\text{RF},t} \mathbf{V}_{\text{BB},t} \in \mathbb{C}^{N \times N_{\text{RF}}}$. Therefore, the post-processed signal at slot t , $\mathbf{y}_t \in \mathbb{C}^{K \times 1}$, is written as

$$\mathbf{y}_t = \sqrt{\beta P_p} \mathbf{V}_t^H \mathbf{h} + \mathbf{V}_t^H \mathbf{n}_t, \quad (53)$$

where $\mathbf{n}_t \sim \mathcal{CN}(\mathbf{0}_{N \times 1}, \sigma^2 \mathbf{I}_N)$ is the additive noise vector. Let $N_{\text{beam}} = N_{\text{slot}} N_{\text{RF}}$ denote the total number of pilot beams. After N_{slot} training slots, the BS acquires the measurement vector $\bar{\mathbf{y}} \triangleq [\mathbf{y}_1^T, \dots, \mathbf{y}_{N_{\text{slot}}}^T]^T \in \mathbb{C}^{N_{\text{beam}} \times 1}$ for \mathbf{h} as

$$\bar{\mathbf{y}} = \sqrt{\beta P_p} \begin{bmatrix} \mathbf{V}_1^H \\ \vdots \\ \mathbf{V}_{N_{\text{slot}}}^H \end{bmatrix} \mathbf{h} + \begin{bmatrix} \mathbf{V}_1^H \mathbf{n}_1 \\ \vdots \\ \mathbf{V}_{N_{\text{slot}}}^H \mathbf{n}_{N_{\text{slot}}} \end{bmatrix} = \sqrt{\beta P_p} \bar{\mathbf{V}}^H \mathbf{h} + \bar{\mathbf{n}}, \quad (54)$$

where $\bar{\mathbf{V}} \triangleq [\mathbf{V}_1, \dots, \mathbf{V}_{N_{\text{slot}}}] \in \mathbb{C}^{N \times N_{\text{beam}}}$, whereas $\bar{\mathbf{n}} \in \mathbb{C}^{N_{\text{beam}} \times 1}$ is the effective noise. More particularly, $\mathbf{R}_{\bar{\mathbf{n}}[s]} \triangleq \sigma^2 \text{blkdiag}(\mathbf{V}_1^H \mathbf{V}_1, \dots, \mathbf{V}_{N_{\text{slot}}}^H \mathbf{V}_{N_{\text{slot}}})$ is the covariance matrix of the effective noise, which is colored in general.⁵ Regarding the pilot combiners, due to the hybrid array architecture, $\bar{\mathbf{V}} = \bar{\mathbf{V}}_{\text{RF}} \bar{\mathbf{V}}_{\text{BB}}$, with $\bar{\mathbf{V}}_{\text{RF}} = [\mathbf{V}_{\text{RF},1}, \dots, \mathbf{V}_{\text{RF},N_{\text{slot}}}] \in \mathbb{C}^{N \times N_{\text{beam}}}$ and $\bar{\mathbf{V}}_{\text{BB}} = \text{blkdiag}(\mathbf{V}_{\text{BB},1}, \dots, \mathbf{V}_{\text{BB},N_{\text{slot}}}) \in \mathbb{C}^{N_{\text{beam}} \times N_{\text{beam}}}$ comprising the pilot RF beams and baseband combiners of the N_{slot} time slots, respectively.

C. Orthogonal Matching Pursuit

1) *Sparse Formulation:* We next consider a dictionary $\bar{\mathbf{H}} \in \mathbb{C}^{N_{\text{beam}} \times G}$ whose G columns are the channel vectors associated with a predefined set of angles-of-arrival (AoA). Then, the uplink channel can be approximated as

$$\mathbf{h} \approx \bar{\mathbf{H}} \boldsymbol{\beta}, \quad (55)$$

where $\boldsymbol{\beta}$ is a $G \times 1$ vector with a single nonzero entry corresponding to the LoS path. Therefore, (54) is recast as $\bar{\mathbf{y}} \approx \bar{\Phi} \boldsymbol{\beta} + \bar{\mathbf{n}}$, where $\bar{\Phi} \triangleq \sqrt{P_p} \bar{\mathbf{V}}^H \bar{\mathbf{H}} \in \mathbb{C}^{N_{\text{beam}} \times G}$ is the *equivalent* sensing matrix. Since $G \gg 1$, the vector $\bar{\boldsymbol{\beta}}$

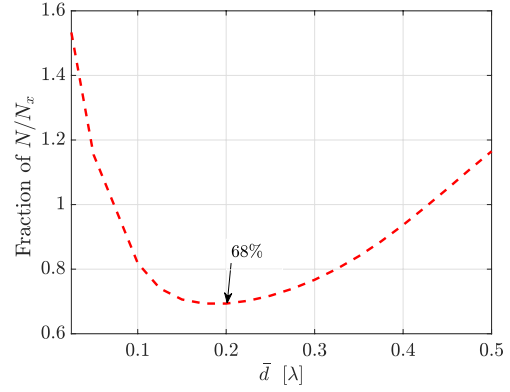


Fig. 7: Fraction of N/N_x versus \bar{d} for $(\theta, \phi) = (0, 0)$ at $f = 300$ GHz. The dipoles are half-wavelength copper wires of radius $\rho = \lambda/500$.

is 1-sparse, and thus the channel estimation problem can be formulated as the sparse recovery problem [46]

$$\hat{\boldsymbol{\beta}} = \arg \min_{\boldsymbol{\beta}} \|\boldsymbol{\beta}\|_1 \quad \text{subject to} \quad \|\bar{\mathbf{y}} - \bar{\Phi} \boldsymbol{\beta}\| \leq \epsilon, \quad (56)$$

where $\epsilon \leq \mathbb{E}\{\|\bar{\mathbf{n}}\|\}$ is an appropriately chosen bound on the mean magnitude of the effective noise. The l_1 -norm optimization problem in (56) can be readily solved by the popular OMP algorithm, which takes the following form for single-path channels

$$g^* = \arg \max_{g \in \mathcal{G}} |\Phi^H(g) \bar{\mathbf{y}}|, \quad (57)$$

where \mathcal{G} denotes the set of predefined AoA. Finally, the estimate of \mathbf{h} is obtained as $\hat{\mathbf{h}} = \bar{\mathbf{H}}(g^*)$. It is worth stressing that the actual AoA might differ from the one defined by the dictionary. Nonetheless, this mismatch error can become negligible by adopting a high-resolution dictionary, as demonstrated in [46].

2) *Dictionary and Pilot Beams:* In the spirit of [47], [48], we discretize the polar angle $\theta \in [0, \theta_{\text{max}}]$ and azimuth angle $\phi \in [0, \phi_{\text{max}}]$ as

$$\bar{\theta}_{g_z} = \frac{\theta_{\text{max}}}{G_z} g_z, \quad g_z = 0, \dots, G_z - 1, \quad (58)$$

$$\bar{\phi}_{g_x} = \frac{\phi_{\text{max}}}{G_x} g_x, \quad g_x = 0, \dots, G_x - 1, \quad (59)$$

where $G = G_x G_z$ is the overall dictionary size, which results in the coupling-aware dictionary

$$\bar{\mathbf{H}} = \left[\text{Re}\{\mathbf{Z}\}^{-\frac{1}{2}} \mathbf{a}(\bar{\theta}_0, \bar{\phi}_0), \dots, \text{Re}\{\mathbf{Z}\}^{-\frac{1}{2}} \mathbf{a}(\bar{\theta}_{G_z-1}, \bar{\phi}_{G_x-1}) \right]. \quad (60)$$

The elements of the RF combiner $\bar{\mathbf{V}}_{\text{RF}}$ are selected from the set $\{-1/\sqrt{N}, 1/\sqrt{N}\}$ with equal probability. The reason we adopt a randomly formed RF combiner is that it will exhibit low mutual-column coherence, and therefore is expected to attain a high recovery probability according to the compressed sensing (CS) theory [49]. The columns of $\bar{\mathbf{V}}_{\text{RF}}$ have been normalized so that the total power consumed during the channel estimation stage is $P_{\text{CE}} = KN_{\text{beam}} P_p$, as KN_{beam} pilot beams are used for the K users. The specific RF pilot design results in a colored effective noise. For this reason, we

⁵We have assumed the same noise variance, σ^2 , as in the user side.

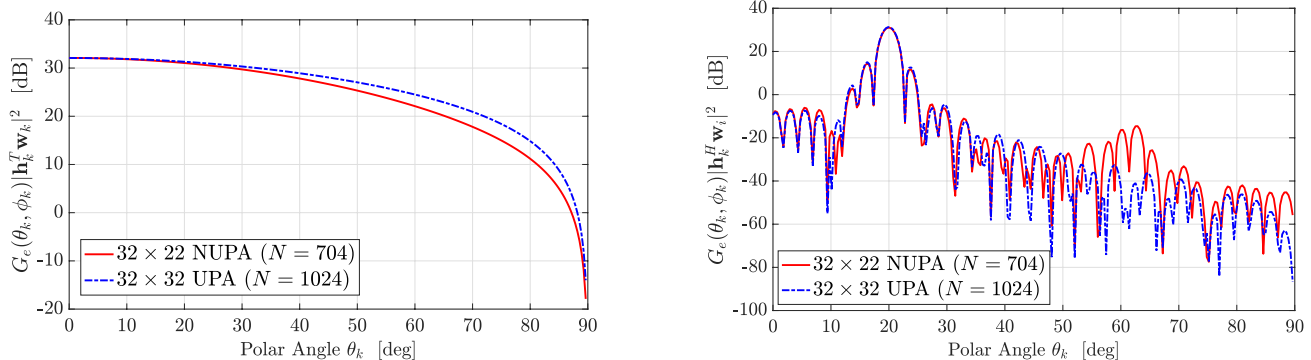


Fig. 8: Signal and interference powers. In NUPA, $\bar{N} = 2$, $N_g = 11$, $d_x = 0.7\lambda$, $\bar{d} = \lambda/5$, and $d_g = 1.95\lambda$. In uniform planar array (UPA), $d = d_x = 0.7\lambda$. The interference power is computed for $(\theta_i, \phi_i) = (20^\circ, 0^\circ)$. Also, $P_t = 1/2$, $K = 1$, and $f = 300$ GHz.

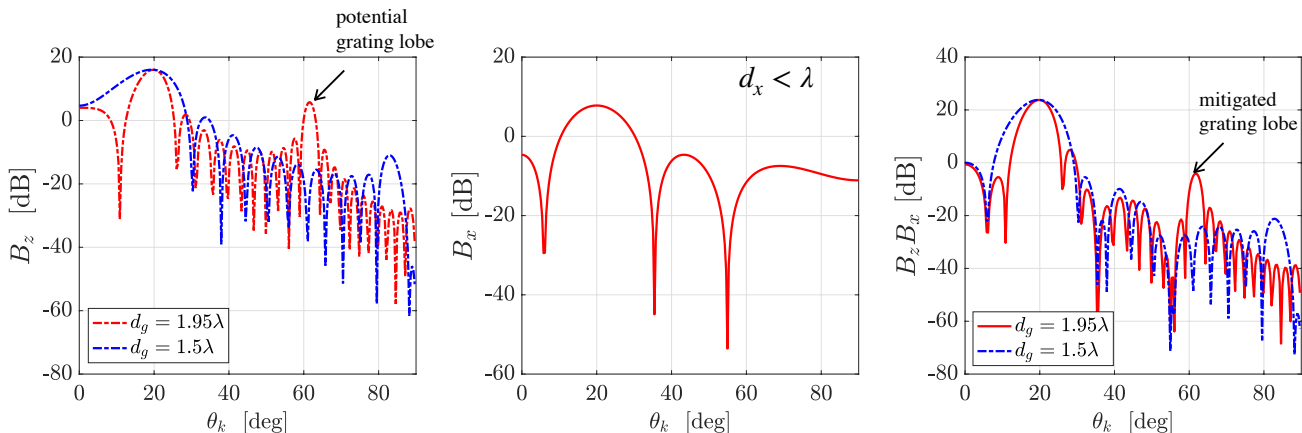


Fig. 9: Polar beampatterns of a 6×22 -element NUPA with $\bar{d} = \lambda/5$, $d_x = 0.7\lambda$, and various d_g . The beamforming angle is $(\theta_i, \phi_i) = (20^\circ, 0^\circ)$.

design the baseband combiner such that the effective noise remains white. Let $\mathbf{D}_t^H \mathbf{D}_t$ be the Cholesky decomposition of $\mathbf{V}_{\text{RF},t}^H \mathbf{V}_{\text{RF},t}$, where $\mathbf{D} \in \mathbb{C}^{N_{\text{RF}} \times N_{\text{RF}}}$ is an upper triangular matrix. Then, the baseband combiner of the t th slot is set to $\mathbf{V}_{\text{BB},t} = \mathbf{D}_t^{-1}$, and hence $\bar{\mathbf{V}} = \bar{\mathbf{V}}_{\text{RF}} \text{blkdiag}(\mathbf{D}_1^{-1}, \dots, \mathbf{D}_{N_{\text{slot}}}^{-1})$. Under this pilot beam design, the covariance matrix of the effective noise becomes $\mathbf{R}_{\bar{\mathbf{n}}} = \sigma^2 \mathbf{I}_{N_{\text{beam}}}$.

VIII. REDUCING THE NUMBER OF BS ANTENNAS

As demonstrated in Section VI-B, the proposed NULA achieves larger gain than ULA thanks to the superdirective pairs. This excessive power gain can improve EE, because the number of antennas is kept fixed in both array designs. A more radical approach is to adopt a NULA with fewer elements than a ULA to substantially reduce the power consumption, akin to the paradigm of array thinning. Hereafter, we focus on the general case of planar arrays, and determine the parameters N_g , d_g , and \bar{d} of NUPA in order to attain a similar signal and interference power as a UPA of N elements.

A. How Many BS Antennas Do We Need?

For the sake of fair comparison, we consider that both NUPA and UPA have N_x elements along the x -axis with

inter-element spacing d_x . We then seek to find how many antennas along the z -axis are needed such that the two arrays offer the same signal power toward the endfire direction $(\theta, \phi) = (0^\circ, 0^\circ)$. This occurs when

$$N_x N_g \mathbf{a}_0^H(0) \text{Re} \{ \bar{\mathbf{Z}}_0 \}^{-1} \mathbf{a}_0(0) = N, \quad (61)$$

which gives, after some basic algebra,

$$2N_g = \frac{1 - \bar{R}_m^2}{(1 - \bar{R}_m \cos(\kappa \bar{d}))} \frac{N}{N_x}. \quad (62)$$

Note that (62) hinges on the inter-element spacing \bar{d} within dipole pairs, which determines the level of mutual coupling. From Fig. 7, we observe that the minimum number of antennas is attained for $\bar{d} = \lambda/5$.⁶ In this case, the NUPA requires approximately 68% of the UPA antennas along the z -axis, and hence up to 32% saving in RF hardware is possible. This performance can be readily obtained for a point-to-point link where the user is placed at the endfire direction of the BS. Conversely, the impact of reducing the number of BS antennas on the performance of multiuser transmissions is hard to analytically study, under either perfect or imperfect CSI. For

⁶For spacings smaller than $\lambda/5$, the ohmic losses become dominant and decrease the array gain.

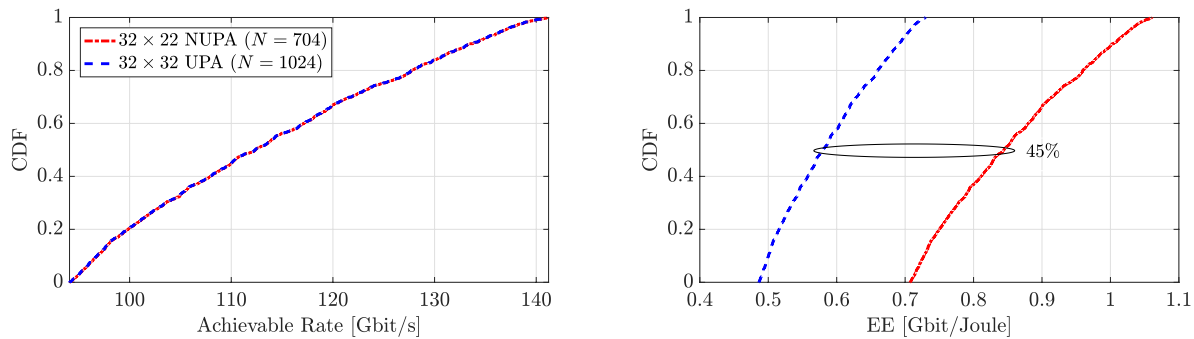


Fig. 10: Results for a point-to-point link. In the NUPA, $\bar{N} = 2$, $N_g = 11$, and $\bar{d} = \lambda/5$.

this reason, we resort to numerical simulations in Section IX. and

B. Spatial Resolution and Inter-Group Spacing

It is known that spatial resolution is determined by the array size [26]. Thus, the NUPA with less elements will preserve its spatial resolution if its length along the z -axis is equal to that of UPA. This happens for $N_g \bar{d} + (N_g - 1)d_g = (N/N_x - 1)d$, or equivalently

$$d_g = \frac{(N/N_x - 1)d - N_g \bar{d}}{N_g - 1}, \quad (63)$$

which ensures that the NUPA and UPA have the same physical size. To demonstrate this design methodology, we consider a 32×32 -element UPA at the BS with $d = d_x = 0.7\lambda$. Then, the NUPA will consist of $N_g = 11$ dipole pairs, yielding a 32×22 -element array with inter-group spacing $d_g = 1.95\lambda$. We now compare these two arrays in terms of the overall signal and interference powers given by $\beta_k |\mathbf{h}_k^T \mathbf{w}_k|^2 \propto G_e(\theta_k, \phi_k) |\mathbf{h}_k^T \mathbf{w}_k|^2$ and $\beta_k |\mathbf{h}_k^T \mathbf{w}_i|^2 \propto G_e(\theta_k, \phi_k) |\mathbf{h}_k^T \mathbf{w}_i|^2$, respectively. From Fig. 8, we verify that both arrays have very similar performance, though the NUPA employs much fewer elements than UPA. Lastly, the side lobes occurred for polar angles θ_k beyond 50° can be neglected since their power is less than 0 dB. About possible grating lobes, these will appear if $d_g + \bar{d} > \lambda$ and $d_x > \lambda$. Their positions, in the polar plane (i.e., $\phi_k = \phi_i = 0$), are given by [26]

$$\theta_k = \cos^{-1} \left(\cos \theta_i \pm n_1 \frac{\lambda}{d_g + \bar{d}} \right) = \sin^{-1} \left(\sin \theta_i \pm n_2 \frac{\lambda}{d_x} \right), \quad (64)$$

for n_1 and n_2 in $\{1, 2, 3, \dots\}$. Since $d_x < \lambda$, (64) does not admit a real solution, and hence grating lobes do not occur in the visible region of the NUPA. In practice, these are suppressed by the low-level sidelobes of the array along the x -axis, as indicated by (52). This behavior is confirmed in Fig. 9, where

$$\begin{aligned} B_z &= G_e(\theta_k, \phi_k) \\ &\times N_g \left| D_{N_g} (\kappa(d_g + (\bar{N} - 1)\bar{d})(\cos \theta_k - \cos \theta_i)) \right|^2 \\ &\times \frac{\left| \mathbf{a}_0^H(\theta_k) \text{Re} \{ \bar{\mathbf{Z}}_0 \}^{-1} \mathbf{a}_0(\theta_i) \right|^2}{\left| \mathbf{a}_0^H(\theta_i) \text{Re} \{ \bar{\mathbf{Z}}_0 \}^{-1} \mathbf{a}_0(\theta_i) \right|^2} \end{aligned} \quad (65)$$

$$B_x = N_x \left| D_{N_x} (\kappa d_x (\cos \phi_k \sin \theta_k - \cos \phi_i \sin \theta_i)) \right|^2 \quad (66)$$

are the beampatterns of the NUPA along the z and x directions, respectively [50].

Remark 2. *The proposed NUPA enables beam broadening without sacrificing the maximum array gain by adopting a small inter-group spacing d_g , i.e., by decreasing the length of the overall array along the z -axis. This feature is showcased in Fig. 9, and can be very useful for THz links where wide beamwidths alleviate the detrimental effect of beam misalignment [51].*

TABLE II
MAIN SIMULATION PARAMETERS [20], [38], [51]

Parameter	Value
Carrier frequency, bandwidth	$f = 300$ GHz, $B = 15$ GHz
BS's input power	$P_t = 20$ dBm
Power per pilot symbol	$P_p = 20$ dBm
Power density of noise	$\sigma^2 = -174$ dBm/Hz
User distance	$r_k \sim \mathcal{U}(5, 15)$ m
Absorption coefficient	$k_{\text{abs}} = 0.0033$ m ⁻¹
Dipole length, radius	$\ell = \lambda/2$, $\rho = \lambda/500$
Copper conductivity	$\sigma_c = 5.7 \times 10^7$ S/m
Baseband unit	$P_{\text{BB}} = 200$ mW
Phase shifter	$P_{\text{PS}} = 42$ mW
Power amplifier	$P_{\text{PA}} = 60$ mW
DAC	$P_{\text{DAC}} = 110$ mW
Local oscillator	$P_{\text{LO}} = 4$ mW
Mixer	$P_{\text{M}} = 22$ mW

IX. SIMULATION RESULTS

We conduct extensive numerical simulations to assess the performance of the proposed array design. In all numerical experiments, we consider a fractional bandwidth $B/f \leq 0.1$ and LoS links, which ensure a spatially narrowband propagation channel [46]. The other simulation parameters are summarized in Table II. Also, all values in the power consumption model are taken from [20].

A. Point-to-Point Link

We commence with the case of a point-to-point link, where a single user is placed at $(\theta, \phi) = (0^\circ, 0^\circ)$. Note that this setup can represent a wireless backhaul link. Due to the fixed user direction, perfect CSI is assumed at the BS.

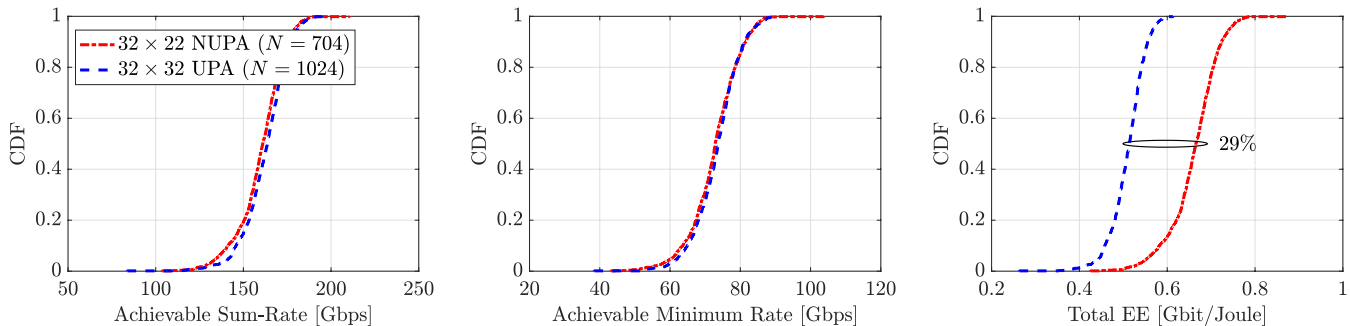


Fig. 11: Results for $K = 2$ users with directions $\theta_k \sim \mathcal{U}(0^\circ, 50^\circ)$ and $\phi_k \sim \mathcal{U}(0^\circ, 360^\circ)$. The BS acquires CSI with partial training of $N_{\text{beam}} = 0.8N$ pilots per user. The dictionary size is $G = N$ for each array design. In NUPA, $\bar{d} = \lambda/5$, $d_g = 1.95\lambda$, and $d_x = 0.7\lambda$. In UPA, $d_x = d = 0.7\lambda$.

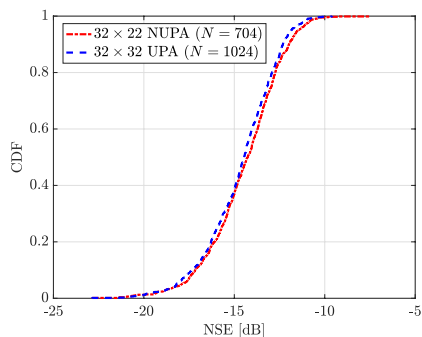


Fig. 12: CDF of the NSE for $K = 2$ users and partial beam training with $N_{\text{beam}} = 0.8N$ pilots per user.

The distance from the BS follows the uniform distribution $\mathcal{U}(5, 15)$ m. The maximum achievable rate and EE are given by $R = B \log_2 \left(1 + \frac{\beta |\mathbf{h}^T \mathbf{w}|^2}{B\sigma^2} \right)$ and R/P_c , respectively. The signal power $|\mathbf{h}^T \mathbf{w}|^2$ is determined by (51) and is independent of d_g and d_x . The cumulative distribution function (CDF) of each metric is calculated for 1,000 channel realizations. From Fig. 10 of the next page, we observe that the NUPA attains the same achievable rate as UPA, yet with 320 antennas less. This translates roughly to 31% saving in RF circuitry, such as power amplifiers, phase shifters and combiners, which in turn yields a mean EE improvement of 45%.

For the point-to-point deployment, we can employ single-port impedance matching as the beamforming angle is kept fixed all the time. Subsequently, we investigate how this is accomplished. To calculate the active impedance of each dipole, the endfire current vector is decomposed as $\mathbf{i}^{\text{opt}} = [\mathbf{i}_0^{\text{opt}}, \dots, \mathbf{i}_{N_g-1}^{\text{opt}}]^T$, where $\mathbf{i}_{n_g}^{\text{opt}} \triangleq [I_{n_g}(0), I_{n_g+1}(0)]^T$ denotes the optimal excitation vector at each antenna pair. This is defined as

$$\begin{aligned} \mathbf{i}_{n_g}^{\text{opt}} &= \frac{\sqrt{2P_t} e^{-j\kappa n_g(d_g + \bar{d})}}{\sqrt{N_g} \mathbf{a}_0^H(0) \text{Re}\{\mathbf{Z}_0\}^{-1} \mathbf{a}_0(0)} \text{Re}\{\mathbf{Z}_0\}^{-1} \mathbf{a}_0(0) \\ &= \frac{\sqrt{P_t} e^{-j\kappa n_g(d_g + \bar{d})}}{\sqrt{N_g} (R_{\text{self}} - R_m \cos(\kappa \bar{d}))} \begin{bmatrix} R_{\text{self}} - R_m e^{-j\kappa \bar{d}} \\ -R_m + R_{\text{self}} e^{-j\kappa \bar{d}} \end{bmatrix}, \end{aligned} \quad (67)$$

where (67) follows from (12) and (45) for $\theta = 0^\circ$. Therefore,

for any pair n_g , we have that

$$\frac{I_{n_g+1}(0)}{I_{n_g}(0)} = \frac{-R_m + R_{\text{self}} e^{-j\kappa \bar{d}}}{R_{\text{self}} - R_m e^{-j\kappa \bar{d}}}, \quad (68)$$

which is independent of the group index n_g . Now let

$$\mathbf{Z}_0 \triangleq \begin{bmatrix} Z_{\text{self}} & Z_m \\ Z_m & Z_{\text{self}} \end{bmatrix}, \quad (69)$$

with $\text{Re}\{Z_{\text{self}}\} = R_{\text{self}}$ and $\text{Re}\{Z_m\} = R_m$. The input impedance matrix \mathbf{Z}_0 is computed by the induced EMF method for two side-by-side dipoles [26, Ch. 8]. Since $\mathbf{Z} = \mathbf{I}_{N_g} \otimes \mathbf{Z}_0$, it is straightforward to prove that $\mathbf{Z}_a = \text{blkdiag}(\mathbf{Z}_{0,a}, \dots, \mathbf{Z}_{0,a})$ using the relationship $\mathbf{Z}_a \mathbf{i}^{\text{opt}} = \mathbf{Z} \mathbf{i}^{\text{opt}}$, where

$$\begin{aligned} \mathbf{Z}_{0,a} &= \begin{bmatrix} Z_{\text{self}} + Z_m \frac{I_{n_g+1}(0)}{I_{n_g}(0)} & 0 \\ 0 & Z_{\text{self}} + Z_m \frac{I_{n_g}(0)}{I_{n_g+1}(0)} \end{bmatrix} \\ &= \begin{bmatrix} Z_{\text{self}} + Z_m \frac{-R_m + R_{\text{self}} e^{-j\kappa \bar{d}}}{R_{\text{self}} - R_m e^{-j\kappa \bar{d}}} & 0 \\ 0 & Z_{\text{self}} + Z_m \frac{R_{\text{self}} - R_m e^{-j\kappa \bar{d}}}{-R_m + R_{\text{self}} e^{-j\kappa \bar{d}}} \end{bmatrix}. \end{aligned} \quad (70)$$

Therefore, all dipole pairs share a common active impedance matrix whose entries are $[\mathbf{Z}_{0,a}]_{1,1} = 21.84 + j32.89 \Omega$, and $[\mathbf{Z}_{0,a}]_{2,2} = 40.87 + j83.89 \Omega$, for half-wavelength dipoles made of copper and inter-element distance $\bar{d} = \lambda/5$. This is a unique feature of the proposed NULA/NUPA. In contrast, a superdirective ULA/UPA would need a different matching impedance for each port because the current amplitude is not uniform along the ports (akin to the source voltages). Thus, the derived architecture simplifies also single-port matching. Finally, compared to an uncoupled ULA/UPA with $Z_{\text{self}} = 75.94 + j41.76 \Omega$, the active impedances $[\mathbf{Z}_{0,a}]_{1,1}$ and $[\mathbf{Z}_{0,a}]_{2,2}$ are not very large, and thus could be easily matched.

B. Multiuser Transmissions with Imperfect CSI

We now consider that the BS simultaneously transmits to K users using MRT. The users' directions are not fixed, and thus the BS acquires the channel estimates $\{\hat{\mathbf{h}}_k\}_{k=1}^K$ through the OMP estimator of Section VII-C. In the UPA case, the dictionary is $\bar{\mathbf{H}} = [\mathbf{a}(\theta_0, \bar{\phi}_0), \dots, \mathbf{a}(\theta_{G_z-1}, \bar{\phi}_{G_z-1})]$. The BS treats those estimates as the true channels in the

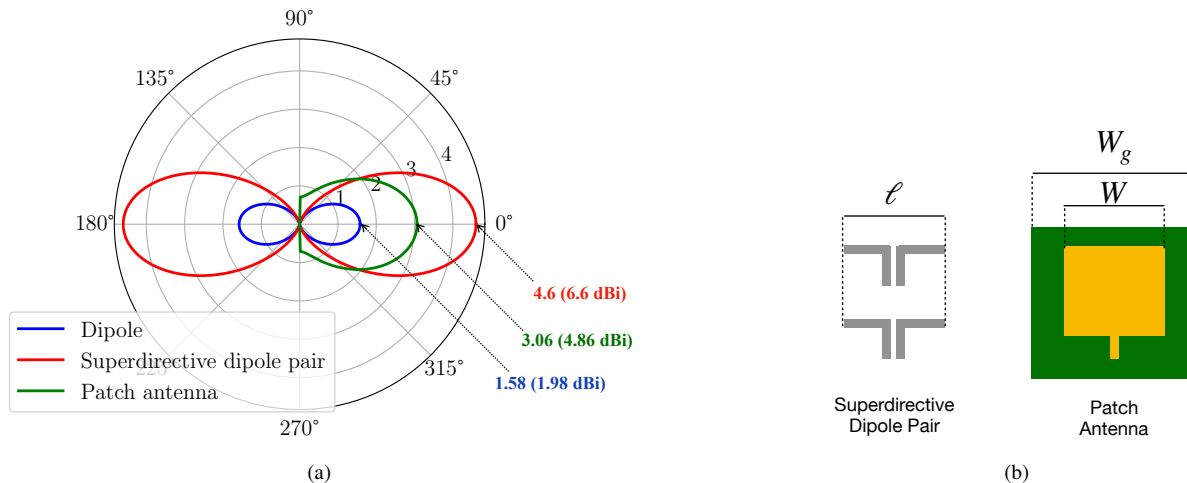


Fig. 13: (a) Gain patterns at the vertical plane $\phi = 0$. The spacing between dipoles is $\bar{d} = \lambda/5$. (b) Sketch of patch antenna and superdirective pair geometries.

beamforming stage, i.e., $\mathbf{w}_k = \hat{\mathbf{h}}_k^* / \|\hat{\mathbf{h}}_k\|$. The achievable rate of user k is then specified as $R_k = B \log_2(1 + \text{SINR}_k)$, where SINR_k is given by (35). Note that this rate is achieved under the assumption that user k knows $|\mathbf{h}_k^T \mathbf{w}_k|^2$ and $\sum_{i \neq k} |\mathbf{h}_k^T \mathbf{w}_i|^2$ in the decoding stage. These are scalars and, hence, are easy to be estimated. For the performance evaluation, the primary metrics are the sum-rate, minimum rate, and total EE defined as $\sum_{k=1}^K R_k$, $\min_k \{R_k\}$, and $\sum_{k=1}^K R_k / P_c$, respectively.

Figure 11 shows the results for a two-user transmission. As observed, the NUPA boosts the mean EE by 29% without compromising the sum or minimum data rate. Regarding the OMP estimator, we calculate the normalized squared error (NSE) defined as $\text{NSE} \triangleq \frac{1}{K} \sum_{k=1}^K \frac{\|\mathbf{h}_k - \hat{\mathbf{h}}_k\|^2}{\|\mathbf{h}_k\|^2}$. The training overhead per user is $N_{\text{beam}} = 0.8N \approx 564$ pilot beams for the NUPA, whilst $N_{\text{beam}} \approx 820$ beams for the UPA. Importantly, Fig. 12 indicates that channel estimation accuracy is similar for both arrays, although the NUPA employs 256 pilots less. Consequently, it has the potential to reduce also the CSI acquisition overhead of massive MIMO BS.

C. Comparison with Patch Antennas

Microstrip antennas, also known as patch antennas, are widely adopted in real-world mmWave and THz MIMO systems due to their planar geometry, directional radiation characteristics, and easy fabrication into printed circuit boards [52]. As such, it is of practical interest to investigate how our superdirective design compares with a typical patch antenna array. Here, we would like to stress that the proposed superdirective pair can be readily realized with printed dipoles in order to have a planar radiating structure [53]. In the sequel, we consider a copper patch of length L and width W on top of a grounded dielectric substrate of thickness h , dielectric constant ϵ_r , and loss tangent $\tan \delta$. To ensure high radiation efficiency, the substrate thickness is selected in the range $0.025\lambda \leq h \leq 0.05\lambda$, where λ is the free-space wavelength. Since the fields generated by the antenna propagate in two

different media, a homogeneous medium is assumed with effective dielectric constant [26]

$$\epsilon_{\text{reff}} = \frac{\epsilon_r + 1}{2} + \frac{\epsilon_r - 1}{2} \frac{1}{\sqrt{1 + 12h/W}}. \quad (71)$$

1) *Antenna Gain*: For the dominant transverse magnetic TM_{010} mode, the width and length of the copper patch are chosen as [26]

$$W = \frac{c}{2f_r} \sqrt{\frac{2}{\epsilon_r + 1}}, \quad (72)$$

and

$$L = \frac{c}{2f_r \sqrt{\epsilon_{\text{reff}}}} - 2\Delta L, \quad (73)$$

where f_r denotes the resonant frequency of the antenna, and

$$\Delta L = 0.412h \frac{(\epsilon_{\text{reff}} + 0.3)(W/h + 0.264)}{(\epsilon_{\text{reff}} - 0.258)(W/h + 0.8)}. \quad (74)$$

Using these equations, the dimensions of the radiator are calculated for given f_r , h , ϵ_r , and $\tan \delta$. Next, the azimuth E_θ and polar E_ϕ components of the electric field of the antenna are specified by [54, Ch. 4]

$$E_\theta = \frac{2h \sin\left(\frac{\pi W}{\lambda} \sin \theta \sin \phi\right)}{\pi \sin \theta \sin \phi} \cos\left(\frac{\pi L_{\text{reff}}}{\lambda} \sin \theta \cos \phi\right) \cos \phi, \quad (75)$$

$$E_\phi = -\frac{2h \sin\left(\frac{\pi W}{\lambda} \sin \theta \sin \phi\right)}{\pi \sin \theta \sin \phi} \times \cos\left(\frac{\pi L_{\text{reff}}}{\lambda} \sin \theta \cos \phi\right) \cos \theta \sin \phi, \quad (76)$$

where $L_{\text{reff}} \triangleq L + \Delta L$ is the effective length. Note that (75)-(76) are valid for polar angles $0 \leq \theta \leq \pi/2$ due to the presence of the ground plane. The directivity of the antenna is defined as $D(\theta, \phi) \triangleq 4\pi U / P_{\text{rad}}$, where $U = \frac{1}{2\eta}(E_\theta^2 + E_\phi^2)$ is the radiation intensity and $P_{\text{rad}} = \int_0^{2\pi} \int_0^{\pi/2} U \sin \theta d\theta d\phi$ is the radiated power.

For sufficiently thin substrate, the surface wave losses can

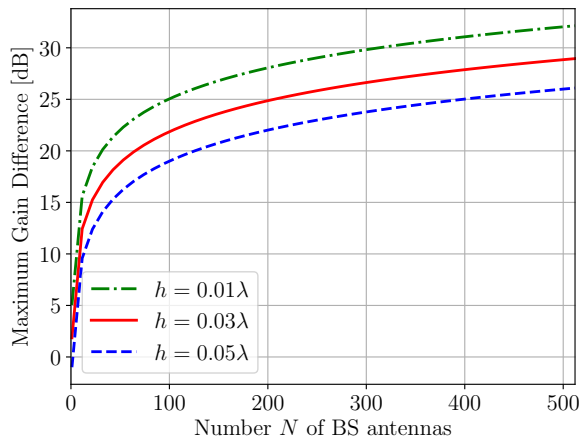


Fig. 14: Broadside gain difference versus the number of BS antennas for various substrate heights.

be neglected, and hence the radiation efficiency is determined by

$$\eta_{\text{rad}} = \frac{P_{\text{rad}}}{P_{\text{rad}} + P_c + P_d}, \quad (77)$$

where P_c and P_d denote the power dissipated in the conducting patch and dielectric substrate, respectively. These are given by the known closed-form expressions [54, Ch. 4]

$$P_d = \frac{1}{4} \omega \epsilon_0 \epsilon_r h L W \tan \delta, \quad (78)$$

$$P_c = \frac{\omega \epsilon_0 \epsilon_r L W}{4 \sigma_c R_s}, \quad (79)$$

where ϵ_0 is the permittivity of free space, ω is the angular frequency, and $R_s = \sqrt{\omega \mu / (2 \sigma_c)}$ is the sheet resistance of the copper patch. Finally, the element gain is $G_e(\theta, \phi) = \eta_{\text{rad}} D(\theta, \phi)$.

Figure 13(a) shows the gain pattern of a single half-wavelength dipole, a superdirective dipole pair, and a rectangular patch antenna with copper and a Polydimethylsiloxane substrate ($\epsilon_r = 2.35, \tan \delta = 0.03$) of thickness $h = 0.03\lambda$ [55]. The estimated patch antenna directivity at broadside is $D(0, 0) = 7.1$ dBi with radiation efficiency $\eta_{\text{rad}} = 60\%$, yielding a maximum gain $G_e(0, 0) = 4.86$ dBi in perfect agreement with [55], [56]. On the other hand, the superdirective dipole pair offers a 6.6 dBi gain, and exhibits sufficient directionality at the element level. Regarding the footprint of the radiators, the width of the patch antenna is determined by the width of the grounded substrate, as depicted in Fig. 13(b), and is given by $W_g = 6h + W \approx 0.56\lambda$ [54]. Therefore, it is slightly larger than that of the half-wavelength dipoles comprising the superdirective pair.

2) *Array Gain*: We now consider a linear array of N elements. Both the superdirective pair and the patch antenna have nulls in the radiation pattern at $\theta = \pi/2$, and hence the elements can be placed in a linear configuration with sub-wavelength spacing and negligible mutual coupling. Therefore, the maximum broadside array gain is $G(0, 0) = G_e(0, 0)N$. Figure 14 shows the broadside gain difference between the patch and superdirective antenna arrays. As seen for $h = 0.03\lambda$, the performance improvement is more than 20 dB for

$N > 100$ antennas. More importantly, this is attained with a compact configuration as the patch antenna array will be $N(W_g - \lambda/2) > 6\lambda$ wider for $N > 100$. Consequently, the proposed grouping architecture can enable the realization of low-profile MIMO transceivers.

X. CONCLUSIONS

In this paper, we introduced the novel concept of superdirective dipole pairs. Specifically, we first derived a comprehensive array model that captures the physics of mutual coupling and ohmic losses of nonideal antennas. Capitalizing on the derived model, we then studied the implementation aspects of superdirectivity, namely the impedance matching and hybrid beamforming problems. To surmount the challenges of superdirective ULAs/UPAs, we proposed to partition the BS array into multiple two-element groups of sub-wavelength spacing. The resulting NULA/NUPA facilitates multi-port impedance matching, which is optimal for any beamforming angle. More importantly, it enables the realization of superdirectivity with a single RF chain per beam. Afterwards, we pursued a performance analysis in terms of achievable rate and EE under perfect and imperfect CSI. To this end, approximate closed-form expressions for the signal and multi-user interference powers were provided under MRT. The channel estimation problem was also addressed by employing OMP along with a coupling-aware dictionary. Numerical results were finally provided demonstrating that the proposed method boosts the EE of THz massive MIMO without compromising the data transmission and channel estimation performances. As a result, arrays of superdirective dipole pairs can be a promising approach for realizing energy-efficient MIMO antennas with sharp beamforming capabilities.

ACKNOWLEDGEMENTS

This project has received funding from the European Research Council (ERC) under the European Union's Horizon 2020 research and innovation programme (grant agreement No. 101001331). The work of H. Q. Ngo was supported by the U.K. Research and Innovation Future Leaders Fellowships under Grant MR/X010635/1.

APPENDIX A

Based on the radiation equations, the electric field is specified as [26, Ch. 3]

$$\mathbf{E}(r, \theta, \phi) = -j\eta \frac{k e^{-j\kappa r}}{4\pi r} (A_\theta \mathbf{e}_\theta + A_\phi \mathbf{e}_\phi), \quad (80)$$

where

$$\begin{aligned} A_\theta &= \int_{-\ell/2}^{\ell/2} I(x') \cos \theta \cos \phi e^{j\kappa x' \cos \phi \sin \theta} dx' \\ &= \frac{I(0) \cos \theta \cos \phi}{\sin(\kappa \ell / 2)} \int_{-\ell/2}^{\ell/2} \sin(\kappa \ell / 2 - \kappa |x'|) e^{j\kappa x' \cos \phi \sin \theta} dx', \end{aligned} \quad (81)$$

and

$$\begin{aligned} A_\phi &= \int_{-\ell/2}^{\ell/2} -I(x') \sin \phi e^{j\kappa x' \cos \phi \sin \theta} dx \\ &= -\frac{I(0) \sin \phi}{\sin(\kappa\ell/2)} \int_{-\ell/2}^{\ell/2} \sin(\kappa\ell/2 - \kappa|x'|) e^{j\kappa x' \cos \phi \sin \theta} dx. \end{aligned} \quad (82)$$

Utilizing the identity [26]

$$\int e^{ax} \sin(\beta x + \gamma) dx = \frac{e^{ax}}{a^2 + \beta^2} [a \sin(\beta x + \gamma) - \beta \cos(\beta x + \gamma)], \quad (83)$$

for $a = j\kappa \cos \phi \sin \theta$, $\beta = \kappa$, and $\gamma = \kappa\ell/2$, and after some algebraic manipulations, we get

$$\begin{aligned} \int_{-\ell/2}^{\ell/2} \sin(\kappa\ell/2 - \kappa|x'|) e^{j\kappa x' \cos \phi \sin \theta} dx &= \\ &= \frac{2 \cos(\kappa\ell/2 \cos \phi \sin \theta) - \cos(\kappa\ell/2)}{\kappa \sin^2 \phi + \cos^2 \phi \cos^2 \theta}. \end{aligned} \quad (84)$$

Combining those equations yields the field expression in (2).

APPENDIX B

The inverse matrix of \mathbf{Z}_0 is

$$\text{Re}\{\mathbf{Z}_0\}^{-1} = \frac{1}{R_{\text{self}}^2 - R_m^2} \begin{bmatrix} R_{\text{self}} & -R_m \\ -R_m & R_{\text{self}} \end{bmatrix}. \quad (85)$$

We now need to calculate the square root of the 2×2 matrix $\text{Re}\{\mathbf{Z}_0\}^{-1}$. To do so, we utilize the lemma [57]

$$\mathbf{A}^{1/2} = \frac{1}{t} \begin{bmatrix} a_{11} + s & a_{12} \\ a_{21} & a_{22} + s \end{bmatrix}, \quad (86)$$

for

$$\mathbf{A} = \begin{bmatrix} a_{11} & a_{12} \\ a_{21} & a_{22} \end{bmatrix}, \quad (87)$$

where $s = \sqrt{a_{11}a_{22} - a_{12}a_{21}}$ and $t = \sqrt{a_{11} + a_{22} + 2s}$. In our case, we have that

$$s = \frac{1}{\sqrt{R_{\text{self}}^2 - R_m^2}}, \quad t = \sqrt{\frac{2R_{\text{self}} + 2\sqrt{R_{\text{self}}^2 - R_m^2}}{R_{\text{self}}^2 - R_m^2}}. \quad (88)$$

Applying (86) to $\text{Re}\{\mathbf{Z}_0\}^{-1}$, and after basic algebra, yields

$$\begin{aligned} \text{Re}\{\mathbf{Z}_0\}^{-1/2} &= \frac{1}{\sqrt{2R_{\text{self}} + 2\sqrt{R_{\text{self}}^2 - R_m^2}}} \\ &\times \begin{bmatrix} \frac{R_{\text{self}}}{\sqrt{R_{\text{self}}^2 - R_m^2}} + 1 & -\frac{R_m}{\sqrt{R_{\text{self}}^2 - R_m^2}} \\ -\frac{R_m}{\sqrt{R_{\text{self}}^2 - R_m^2}} & \frac{R_{\text{self}}}{\sqrt{R_{\text{self}}^2 - R_m^2}} + 1 \end{bmatrix}, \end{aligned} \quad (89)$$

and

$$\begin{aligned} \text{Re}\{\mathbf{Z}_0\}^{-1/2} \mathbf{a}_0(\theta) &= \frac{1}{\sqrt{2R_{\text{self}} + 2\sqrt{R_{\text{self}}^2 - R_m^2}}} \\ &\times \begin{bmatrix} \frac{R_{\text{self}}}{\sqrt{R_{\text{self}}^2 - R_m^2}} + 1 - \frac{R_m}{\sqrt{R_{\text{self}}^2 - R_m^2}} e^{-j\kappa\bar{d} \cos \theta} \\ -\frac{R_m}{\sqrt{R_{\text{self}}^2 - R_m^2}} + \left(\frac{R_{\text{self}}}{\sqrt{R_{\text{self}}^2 - R_m^2}} + 1 \right) e^{-j\kappa\bar{d} \cos \theta} \end{bmatrix}. \end{aligned} \quad (90)$$

Lastly, calculating the magnitudes of the entries of $\text{Re}\{\mathbf{Z}_0\}^{-1/2} \mathbf{a}_0(\theta)$, and some algebraic manipulations, we

obtain (31). Also, because $\mathbf{Z} \approx \mathbf{I}_{N_g} \otimes \mathbf{Z}_0$ in the proposed NULA, (18) becomes

$$\mathbf{Z}_M = \begin{bmatrix} -j\text{Im}\{Z_s\} \mathbf{I}_{N_g} \otimes \mathbf{I}_2 & -j\sqrt{R_s} \mathbf{I}_{N_g} \otimes \text{Re}\{\mathbf{Z}_0\}^{1/2} \\ -j\sqrt{R_s} \mathbf{I}_{N_g} \otimes \text{Re}\{\mathbf{Z}_0\}^{1/2} & -j\mathbf{I}_{N_g} \otimes \text{Im}\{\mathbf{Z}_0\} \end{bmatrix}. \quad (91)$$

We now partition the vectors of voltages and currents at the input and output of the impedance matching network as $\mathbf{v}_M = [\mathbf{v}_{M,0}, \dots, \mathbf{v}_{M,N_g-1}]^T$, $\mathbf{i}_M = [\mathbf{i}_{M,0}, \dots, \mathbf{i}_{M,N_g-1}]^T$, $\mathbf{v} = [\mathbf{v}_0, \dots, \mathbf{v}_{N_g-1}]^T$, and $\mathbf{i} = [\mathbf{i}_0, \dots, \mathbf{i}_{N_g-1}]^T$, where $\mathbf{v}_{M,n_g} = [v_{M,n_g}, v_{M,n_g+1}]^T$ is the vector of voltages at the n_g th input port pair; \mathbf{i}_{M,n_g} , \mathbf{v}_{n_g} , and \mathbf{i}_{n_g} are defined similarly. By using (91) and the previous decompositions, (16) is recast as

$$\begin{aligned} \begin{bmatrix} \mathbf{v}_{M,0} \\ \mathbf{v}_0 \end{bmatrix} \dots \begin{bmatrix} \mathbf{v}_{M,N_g-1} \\ \mathbf{v}_{N_g-1} \end{bmatrix}^T &= \\ &= \begin{bmatrix} \mathbf{Z}_{M,0} & \mathbf{I}_{M,0} \\ & -\mathbf{i}_0 \end{bmatrix} \dots \mathbf{Z}_{M,0} \begin{bmatrix} \mathbf{i}_{M,N_g-1} \\ -\mathbf{i}_{N_g-1} \end{bmatrix}^T, \end{aligned} \quad (92)$$

which shows that \mathbf{Z}_M comprises N_g four-port matching networks, which are independent of each other.

APPENDIX C

We have that

$$\begin{aligned} &\frac{|\mathbf{a}^H(\theta_k) \text{Re}\{\bar{\mathbf{Z}}_{\text{approx}}\}^{-1} \mathbf{a}(\theta_i)|^2}{\mathbf{a}^H(\theta_i) \text{Re}\{\bar{\mathbf{Z}}_{\text{approx}}\}^{-1} \mathbf{a}(\theta_i)} \\ &= \frac{|\mathbf{a}_g^H(\theta_k) \otimes \mathbf{a}_0^H(\theta_k) (\mathbf{I}_{N_g} \otimes \text{Re}\{\bar{\mathbf{Z}}_0\}^{-1}) (\mathbf{a}_g(\theta_i) \otimes \mathbf{a}_0(\theta_i))|^2}{(\mathbf{a}_g^H(\theta_i) \otimes \mathbf{a}_0^H(\theta_i)) (\mathbf{I}_{N_g} \otimes \text{Re}\{\bar{\mathbf{Z}}_0\}^{-1}) (\mathbf{a}_g(\theta_i) \otimes \mathbf{a}_0(\theta_i))} \\ &= \frac{|\mathbf{a}_0^H(\theta_k) \text{Re}\{\bar{\mathbf{Z}}_0\}^{-1} \mathbf{a}_0(\theta_i)|^2 |\mathbf{a}_g^H(\theta_k) \mathbf{a}_g(\theta_i)|^2}{\mathbf{a}_0^H(\theta_i) \text{Re}\{\bar{\mathbf{Z}}_0\}^{-1} \mathbf{a}_0(\theta_i) N_g}, \end{aligned} \quad (93)$$

where the identity $(\mathbf{A} \otimes \mathbf{B})(\mathbf{C} \otimes \mathbf{D}) = (\mathbf{AC}) \otimes (\mathbf{BD})$ has been applied twice. Lastly,

$$\begin{aligned} &\frac{|\mathbf{a}_g^H(\theta_k) \mathbf{a}_g(\theta_i)|^2}{N_g} = \frac{1}{N_g} \left| \sum_{n_g=0}^{N_g-1} e^{-j\kappa n_g (d_g + (\bar{N}-1)\bar{d}) (\cos \theta_k - \cos \theta_i)} \right|^2 \\ &= \frac{1}{N_g} \left| \frac{1 - e^{-j\kappa N_g (d_g + (\bar{N}-1)\bar{d}) (\cos \theta_k - \cos \theta_i)}}{1 - e^{-j\kappa (d_g + (\bar{N}-1)\bar{d}) (\cos \theta_k - \cos \theta_i)}} \right|^2 \end{aligned} \quad (94)$$

$$= N_g |D_{N_g}(\kappa(d_g + (\bar{N}-1)\bar{d})(\cos \theta_k - \cos \theta_i))|^2, \quad (95)$$

which completes the proof.

REFERENCES

- [1] W. Roh *et al.*, "Millimeter-wave beamforming as an enabling technology for 5G cellular communications: Theoretical feasibility and prototype results," *IEEE Commun. Mag.*, vol. 52, no. 2, pp. 106-113, Feb. 2014.
- [2] S. D. Assimonis, M. A. B. Abbasi, V. Fusco, "Millimeter-wave multi-mode circular antenna array for uni-cast multi-cast and OAM communication," *Sci. Rep.* 11, 4928, 2021.
- [3] T. S. Rappaport *et al.*, "Wireless communications and applications above 100 GHz: Opportunities and challenges for 6G and beyond," *IEEE Access*, vol. 7, pp. 78729-78757, 2019.
- [4] M. Matthaiou *et al.*, "The road to 6G: Ten physical layer challenges for communications engineers," *IEEE Commun. Mag.*, vol. 59, no. 1, pp. 64-69, Jan. 2021.

- [5] J. Zhang *et al.*, "Prospective multiple antenna technologies for beyond 5G," *IEEE J. Sel. Areas Commun.*, vol. 38, no. 8, pp. 1637–1660, Aug. 2020.
- [6] H. J. Song and N. Lee, "Terahertz communications: Challenges in the next decade," *IEEE Trans. THz Sci. Technol.*, vol. 12, no. 2, pp. 105–117, Mar. 2022.
- [7] E. Björnson, L. Sanguinetti, J. Hoydis, and M. Debbah, "Optimal design of energy-efficient multi-user MIMO systems: Is massive MIMO the answer?," *IEEE Trans. Wireless Commun.*, vol. 14, no. 6, pp. 3059–3075, Jun. 2015.
- [8] O. E. Ayach, R. W. Heath, Jr., S. Abu-Surra, S. Rajagopal, and Z. Pi, "The capacity optimality of beam steering in large millimeter wave MIMO systems," in *Proc. IEEE SPAWC*, Jun. 2012, pp. 100–104.
- [9] A. Uzkov, "An approach to the problem of optimum directive antenna design," *Comptes Rendus (Doklady) de l'Academie des Sci. de l'URSS*, vol. 53, no. 1, pp. 35–38, 1946.
- [10] T. L. Marzetta, "Super-directive antenna arrays: Fundamentals and new perspectives," in *Proc. IEEE ACSSC*, 2019, pp. 1–4.
- [11] L. Han, H. Yin, and T. L. Marzetta, "Coupling matrix-based beamforming for superdirective antenna arrays," in *Proc. IEEE ICC*, 2022, pp. 5159–5164.
- [12] M. L. Morris *et al.*, "Superdirectivity in MIMO systems," *IEEE Trans. Antennas Propag.*, vol. 53, no. 9, pp. 2850–2857, Sept. 2005.
- [13] N. W. Bikhazi and M. A. Jensen, "The relationship between antenna loss and superdirectivity in MIMO systems," *IEEE Trans. Wireless Commun.*, vol. 6, no. 5, pp. 1796–1802, May 2007.
- [14] R. J. Williams, E. de Carvalho, and T. L. Marzetta, "A communication model for large intelligent surfaces," in *Proc. IEEE ICC*, Jun. 2020.
- [15] A. S. Y. Poon and D. N. C. Tse, "Does superdirectivity increase the degrees of freedom in wireless channels?," in *Proc. IEEE ISIT*, Jun. 2015, pp. 1232–1236.
- [16] A. Haskou, A. Sharaiha, and S. Collardey, "Design of small parasitic loaded superdirective end-fire antenna arrays," *IEEE Trans. Antennas Propag.*, vol. 63, no. 12, pp. 5456–5464, Dec. 2015.
- [17] T. Lonsky, J. Kracek, and P. Hazdra, "Superdirective linear dipole array optimization," *IEEE Antennas Wireless Propag. Lett.*, vol. 19, no. 6, pp. 902–906, Jun. 2020.
- [18] C. Lin and G. Y. L. Li, "Terahertz communications: An array-of-subarrays solution," *IEEE Commun. Mag.*, vol. 54, no. 12, pp. 124–131, Dec. 2016.
- [19] H. Li, M. Li, and Q. Liu, "Hybrid beamforming with dynamic subarrays and low-resolution PSs for mmWave MU-MISO systems," *IEEE Trans. Commun.*, vol. 68, no. 1, pp. 602–614, Jan. 2020.
- [20] L. Yan, C. Han, and J. Yuan, "A dynamic array-of-subarrays architecture and hybrid precoding algorithms for terahertz wireless communications," *IEEE J. Sel. Areas Commun.*, vol. 38, no. 9, pp. 2041–2056, Sept. 2020.
- [21] L. Zakrajsek *et al.*, "Design of graphene-based plasmonic nano-antenna arrays in the presence of mutual coupling," in *Proc. EuCAP*, 2017, pp. 1381–1385.
- [22] C. Han, J. M. Jornet, and I. Akyildiz, "Ultra-massive MIMO channel modeling for graphene-enabled terahertz-band communications," in *Proc. IEEE VTC Spring*, 2018, pp. 1–5.
- [23] K. Dovelos, S. D. Assimonis, H. Q. Ngo, B. Bellalta, and M. Matthaiou, "Intelligent reflecting surfaces at terahertz bands: Channel modeling and analysis," in *Proc. IEEE ICC*, Jun. 2021, pp. 1–6.
- [24] Z. Chen *et al.*, "Intelligent reflecting surface assisted terahertz communications toward 6G," *IEEE Wireless Commun.*, vol. 28, no. 6, pp. 110–117, Dec. 2021.
- [25] R. Goossens and H. Rogier, "Optimal beamforming in the presence of mutual coupling," in *Proc. IEEE SCVT*, Nov. 2006, pp. 13–18.
- [26] C. A. Balanis, *Antenna Theory: Analysis and Design*, 3rd ed., John Wiley & Sons, 2012.
- [27] M. T. Ivrlač and J. A. Nossek, "High-efficiency super-gain antenna arrays," in *Proc. Int. ITG WSA*, Feb. 2010, pp. 369–374.
- [28] Y. Fei, Y. Fan, B. K. Lau, and J. S. Thompson, "Optimal single-port matching impedance for capacity maximization in compact MIMO arrays," *IEEE Trans. Antennas Propag.*, vol. 56, no. 11, pp. 3566–3575, Nov. 2008.
- [29] M. T. Ivrlač and J. A. Nossek, "Toward a circuit theory of communication," *IEEE Trans. Circuits Syst.*, vol. 57, no. 7, pp. 1663–1683, Jul. 2010.
- [30] D. M. Pozar, *Microwave Engineering*, John Wiley & Sons, 2009.
- [31] M. T. Ivrlač and J. A. Nossek, "The multiport communication theory," *IEEE Circuits Syst. Mag.*, vol. 14, no. 3, pp. 27–44, Aug. 2014.
- [32] S. Shen and R. D. Murch, "Impedance matching for compact multiple antenna systems in random RF fields," *IEEE Trans. Antennas Propag.*, vol. 64, no. 2, pp. 820–825, Feb. 2016.
- [33] T. Laas, J. A. Nossek, and W. Xu, "Limits of transmit and receive array gain in massive MIMO," in *Proc. IEEE WCNC*, May 2020.
- [34] S. D. Assimonis, T. V. Yioultis, and C. S. Antonopoulos, "Design and optimization of uniplanar EBG structures for low profile antenna applications and mutual coupling reduction," *IEEE Trans. Antennas Propag.*, vol. 60, no. 10, pp. 4944–4949, Oct. 2012.
- [35] X. Yang *et al.*, "Hardware-constrained millimeter-wave systems for 5G: Challenges, opportunities, and solutions," *IEEE Commun. Mag.*, vol. 57, no. 1, pp. 44–50, Jan. 2019.
- [36] X. Gao *et al.*, "Fast channel tracking for terahertz beamspace massive MIMO systems," *IEEE Trans. Veh. Technol.*, vol. 66, no. 7, pp. 5689–5696, Jul. 2017.
- [37] C. Lin and G. Y. Li, "Indoor terahertz communications: How many antenna arrays are needed?," *IEEE Trans. Wireless Commun.*, vol. 14, no. 6, pp. 3097–3107, Jun. 2015.
- [38] C. Han, A. O. Bicen, and I. F. Akyildiz, "Multi-ray channel modeling and wideband characterization for wireless communications in the terahertz band," *IEEE Trans. Wireless Commun.*, vol. 14, no. 5, pp. 2402–2412, May 2015.
- [39] L. N. Ribeiro, S. Schwarz, M. Rupp, and A. L. F. de Almeida, "Energy efficiency of mmWave massive MIMO precoding with low-resolution DACs," *IEEE J. Sel. Topics Signal Process.*, vol. 12, no. 2, pp. 298–312, May 2018.
- [40] E. Björnson, J. Hoydis, and L. Sanguinetti, *Massive MIMO Networks: Spectral, Energy, and Hardware Efficiency*, Foundations and Trends in Signal Processing: vol. 11, no. 3–4, pp. 154–655, 2017.
- [41] M. T. Ivrlač and J. A. Nossek, "Physical modeling of communication systems in information theory," in *Proc. IEEE ISIT*, Jul. 2009, pp. 2179–2183.
- [42] M. Jensen and J. Wallace, "A review of antennas and propagation for MIMO wireless communications," *IEEE Trans. Antennas Propag.*, vol. 52, no. 11, pp. 2810–2824, Nov. 2004.
- [43] C. Hermosilla, R. Feick, R. A. Valenzuela, and L. Ahumada, "Improving MIMO capacity with directive antennas for outdoor-indoor scenarios," in *Proc. IEEE VTC*, May 2008, pp. 414–41.
- [44] T. L. Marzetta, E. G. Larsson, H. Yang, and H. Q. Ngo, *Fundamentals of Massive MIMO*. Cambridge, U.K.: Cambridge Univ. Press, 2016.
- [45] T. Laas, J. A. Nossek, S. Bazzi and W. Xu, "On reciprocity in physically consistent TDD systems with coupled antennas," *IEEE Trans. Wireless Commun.*, vol. 19, no. 10, pp. 6440–6453, Oct. 2020.
- [46] K. Dovelos, M. Matthaiou, H. Q. Ngo, and B. Bellalta, "Channel estimation and hybrid combining for wideband terahertz massive MIMO systems," *IEEE J. Sel. Areas Commun.*, vol. 39, no. 6, pp. 1604–1620, Jun. 2021.
- [47] J. Lee, G.-T. Gil, and Y. H. Lee, "Exploiting spatial sparsity for estimating channels of hybrid MIMO systems in millimeter wave communications," in *Proc. IEEE GLOBECOM*, Dec. 2014, pp. 3326–3331.
- [48] O. E. Ayach, S. Rajagopal, S. Abu-Surra, Z. Pi, and R. W. Heath, Jr., "Spatially sparse precoding in millimeter wave MIMO systems," *IEEE Trans. Wireless Commun.*, vol. 13, no. 3, pp. 1499–1513, Mar. 2014.
- [49] J. A. Tropp and A. C. Gilbert, "Signal recovery from random measurements via orthogonal matching pursuit," *IEEE Trans. Inf. Theory*, vol. 53, no. 12, pp. 4655–4666, Dec. 2007.
- [50] T. J. Brockett and Y. Rahmat-Samii, "Subarray design diagnostics for the suppression of undesirable grating lobes," *IEEE Trans. Antennas Propag.*, vol. 60, no. 3, pp. 1373–1380, Mar. 2012.
- [51] V. Petrov, D. Moltchanov, Y. Koucheryavy, and J. M. Jornet, "Capacity and outage of terahertz communications with user micro-mobility and beam misalignment," *IEEE Trans. Veh. Technol.*, vol. 69, no. 6, pp. 6822–6827, Jun. 2020.
- [52] Y. He, Y. Chen, L. Zhang, S. -W. Wong, and Z. N. Chen, "An overview of terahertz antennas," *China Commun.*, vol. 17, no. 7, pp. 124–165, Jul. 2020.
- [53] B. G. Duffley, G. A. Morin, M. Mikavica, and Y. M. M. Antar, "A wide-band printed double-sided dipole array," *IEEE Trans. Antennas Propag.*, vol. 52, no. 2, pp. 628–631, Feb. 2004.
- [54] R. Garg, P. Bhartia, I. Bahl, and A. Ittipiboon, *Microstrip Antenna Design Handbook*, Artech House, 2001.
- [55] K. R. Jha and S. K. Sharma, "Waveguide integrated microstrip patch antenna at THz frequency," in *Proc. IEEE APSURSI*, 2014, pp. 1851–1852.
- [56] S. Abu-Surra *et al.*, "End-to-end 6G terahertz wireless platform with adaptive transmit and receive beamforming," in *Proc. IEEE ICC Workshops*, 2022, pp. 897–903.
- [57] B. W. Levinger, "The square root of a 2×2 matrix," *Mathematics Mag.*, vol. 53, no. 4, pp. 222–224, 1980.



Konstantinos Dovelos received the Diploma (M.Eng.) degree in electrical and computer engineering from the Aristotle University of Thessaloniki, Greece, in 2016, and the Ph.D. degree from Universitat Pompeu Fabra, Spain, in 2021. From September 2021 through September 2022, he was with the Centre for Wireless Innovation (CWI) at Queen's University Belfast, U.K., working as a Postdoctoral Research Fellow. He is currently an R&D Engineer at Meta Materials Inc., Greece. His research interests span massive MIMO architectures, superdirectivity,

antennas, metasurfaces, and electromagnetic information theory.



Stylianos D. Assimonis received his Diploma (5 years) and Ph.D. degrees in Electrical and Computer Engineering from Aristotle University of Thessaloniki, Greece. Currently, he holds the position of Lecturer (Assistant Professor) at the School of Electronics, Electrical Engineering and Computer Science in Queen's University, Belfast, UK. His primary research interests encompass Electromagnetic Periodic Structures (including metasurfaces and reconfigurable intelligent surfaces), RF Engineering (wireless sensing, Internet of Things (IoT), and RF

Energy Harvesting), and Antennas (spanning super-directive antennas, electrically small antennas, millimeter-wave (mm-Wave) antennas, and electronically steerable parasitic array radiator (ESPAR) antennas).

Dr. Assimonis was honored with the Post-Doctoral Scholarship for Excellence by the Research Committee of Aristotle University of Thessaloniki and by the Centre for Wireless Innovation (CWI) at Queen's University Belfast, UK, in 2012 and 2016, respectively. He has co-authored numerous research papers in the fields of Electromagnetics and RF Engineering, some of which have received distinguished paper awards at prominent events such as Metamaterials 2013, the 2014 IEEE RFID-TA, and the 2015 5th COST IC1301 Workshop. He currently serves as an Editor for Nature Scientific Reports and the MDPI Journal of Low Power Electronics and Applications. In 2019 and 2021, he acted as a Guest Editor for the MDPI Journal of Low Power Electronics and Applications and the MDPI Sensors, respectively.



Hien Quoc Ngo is currently a Reader with Queen's University Belfast, U.K. His main research interests include massive MIMO systems, cell-free massive MIMO, reconfigurable intelligent surfaces, physical layer security, and cooperative communications. He has co-authored many research papers in wireless communications and co-authored the Cambridge University Press textbook *Fundamentals of Massive MIMO* (2016).

He received the IEEE ComSoc Stephen O. Rice Prize in 2015, the IEEE ComSoc Leonard G. Abraham Prize in 2017, and the Best Ph.D. Award from EURASIP in 2018. He also received the IEEE Sweden VT-COM-IT Joint Chapter Best Student Journal Paper Award in 2015. He was awarded the UKRI Future Leaders Fellowship in 2019. He serves as the Editor for the IEEE Transactions on Wireless Communications, IEEE Transactions on Communications, the Digital Signal Processing, and the Physical Communication (Elsevier). He was a Guest Editor of IET Communications, and a Guest Editor of IEEE ACCESS in 2017.



Michail Matthaiou (Fellow, IEEE) was born in Thessaloniki, Greece in 1981. He obtained the Diploma degree (5 years) in Electrical and Computer Engineering from the Aristotle University of Thessaloniki, Greece in 2004. He then received the M.Sc. (with distinction) in Communication Systems and Signal Processing from the University of Bristol, U.K. and Ph.D. degrees from the University of Edinburgh, U.K. in 2005 and 2008, respectively. From September 2008 through May 2010, he was with the Institute for Circuit Theory and Signal

Processing, Munich University of Technology (TUM), Germany working as a Postdoctoral Research Associate. He is currently a Professor of Communications Engineering and Signal Processing and Deputy Director of the Centre for Wireless Innovation (CWI) at Queen's University Belfast, U.K. after holding an Assistant Professor position at Chalmers University of Technology, Sweden. His research interests span signal processing for wireless communications, beyond massive MIMO, intelligent reflecting surfaces, mm-wave/THz systems and deep learning for communications.

Dr. Matthaiou and his coauthors received the IEEE Communications Society (ComSoc) Leonard G. Abraham Prize in 2017. He currently holds the ERC Consolidator Grant BEATRICE (2021-2026) focused on the interface between information and electromagnetic theories. He was awarded the prestigious 2018/2019 Royal Academy of Engineering/The Leverhulme Trust Senior Research Fellowship and also received the 2019 EURASIP Early Career Award. His team was also the Grand Winner of the 2019 Mobile World Congress Challenge. He was the recipient of the 2011 IEEE ComSoc Best Young Researcher Award for the Europe, Middle East and Africa Region and a co-recipient of the 2006 IEEE Communications Chapter Project Prize for the best M.Sc. dissertation in the area of communications. He has co-authored papers that received best paper awards at the 2018 IEEE WCSP and 2014 IEEE ICC. In 2014, he received the Research Fund for International Young Scientists from the National Natural Science Foundation of China. He is currently the Editor-in-Chief of Elsevier Physical Communication, a Senior Editor for IEEE WIRELESS COMMUNICATIONS LETTERS and IEEE SIGNAL PROCESSING MAGAZINE, and an Associate Editor for IEEE TRANSACTIONS ON COMMUNICATIONS. He is an IEEE Fellow.